Magnetic resonance spectroscopy

CHRISTOPHER J. RHODES

Professor Chris Rhodes is Director of Fresh-lands Environmental Actions (www.fresh-lands.com). He has catholic scientific interests which cover radiation chemistry, catalysis, zeolites, radioisotopes, free radicals and electron spin resonance spectroscopy, and more recently have developed into aspects of environmental decontamination and the production of sustainable fuels. Chris has given numerous radio and televised interviews concerning environmental issues. E-mail: cjrhodes@freshlands.com

ABSTRACT

Since the original observation by Zeeman, that spectral lines can be affected by magnetic fields, 'magnetic spectroscopy' has evolved into the broad arsenal of techniques known as 'magnetic resonance'. This review focuses on nuclear magnetic resonance (NMR), electron paramagnetic resonance (EPR), and muon spin resonance (μSR): methods which have provided unparalleled insight into the structures, reactivity and dynamics of molecules, and thereby contributed to a detailed understanding of important aspects of chemistry, and the materials, biomedical, and environmental sciences. Magnetic resonance imaging (MRI), in vivo magnetic resonance spectroscopy (MRS) and functional magnetic resonance spectroscopy (fMRS) are also described. EPR is outlined as a principal method for investigating free radicals, along with biomedical applications, and mention is given to the more recent innovation of pulsed EPR techniques. In the final section of the article, the various methods known as μSR are collected under the heading 'muon spin resonance', in order to emphasise their complementarity with the more familiar NMR and EPR.

Keywords: *nuclear magnetic resonance, NMR, electron paramagnetic resonance, EPR, electron spin resonance, ESR, relaxation, spin-label, coupling, magnetic resonance imaging, MRI, in vivo magnetic resonance spectroscopy, MRS, muon spin resonance, μSR*

1. Introduction

Writing on "The Nature of Sun-Spots" in the 1917–1918 volume (XII) of *Science Progress*[1], the Rev. A.L. Cortie (SJ, FRAS), of Stonyhurst College Observatory, notes that:

"In the year 1896, Prof. Zeeman had demonstrated a new relation between light and magnetism, by proving that the emission and absorption of luminous radiations are modified, when exposed to the influence of magnetic forces. He experimented with a flame containing sodium vapour, which was placed between the poles of a strong electromagnet. The effect produced was that when the current was passed through the coils of the magnet, the D lines of sodium, a double yellow line in a spectroscope of sufficiently high dispersive power, were seen to be widened. Subsequent experiments showed that nearly every radiation observed in a powerful spectroscope is split into three components when the original radiations are observed in a direction at right angles to the lines of force. When, however, the lines are observed along the lines of force, the central line of the triplet disappears, and the two terminal lines remain which are found to be circularly polarised in opposite directions. With suitable polarising apparatus one or other of the two components of the double can be quenched, leaving the other unchanged."

It was on the basis of such measurements of the effects of magnetic fields on the spectral lines[2,3,4] (the 'Zeeman effect') from various elements that the existence of magnetic fields in sunspots (Figure 1) was established[5], at the Mount Wilson Solar Laboratory, by Professor George Ellery Hale, and it was determined that their intensity can be as high as 4,500 gauss[6], (0.45 tesla) or about 9,000 times that of the Earth's magnetic field. In the intervening 100 years, interest in spectroscopy using magnetic fields has acquired a more strongly terrestrial basis, having evolved into the suite of techniques that are collectively termed 'magnetic resonance'. Under this broad heading we may list: nuclear magnetic resonance (NMR)[7], electron paramagnetic resonance (EPR)[8] (formerly, and sometimes alternatively termed electron spin resonance [ESR]), muon spin resonance (μSR)[9], and the multiplicity of sub-methods that are attendant to each of them. (Nuclear) magnetic resonance imaging (MRI) is probably the best known of the magnetic resonance techniques, since it is popularly familiar in hospitals as an alternative to the use of X-rays – typically as a computed tomography (CT) scan – for looking inside the human body. The definite observation of NMR was first reported[10] in 1938, by Isidor Rabi and his co-workers, working at Columbia University on molecular beam experiments. Rabi used an extended version of the Stern–Gerlach apparatus, and made the critical discovery that an oscillating (radiofrequency) magnetic field could impel transitions to occur between different nuclear magnetic moment states. Rabi won the Nobel Prize for Physics in 1944[11] for his resonance method for recording the magnetic properties of atomic nuclei. Felix Bloch (Standard University) and Edward Mills Purcell (Harvard University) extended the use of NMR to liquids and solids, and were jointly awarded the Nobel Prize in Physics in 1952[12] for their development of new methods for nuclear magnetic precision measurements and discoveries in connection therewith. It is believed that the Russian physicist, Yevgeny Zavoisky probably observed NMR in 1941, but he did not consider the results as reproducible and dismissed them. However, credit is given to Zavoisky for the first observation of EPR at Kazan State University in 1944, published in 1945[13].
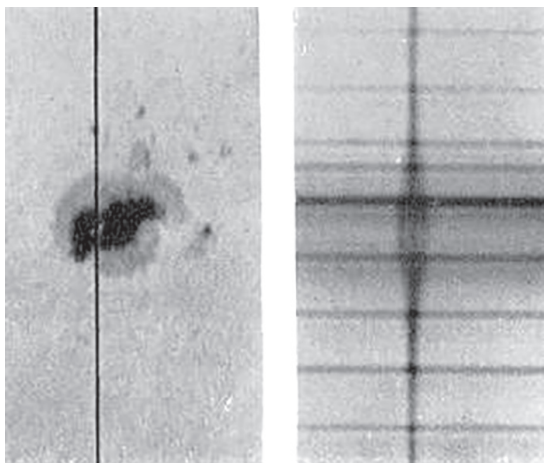
Figure 1 *Magnetic field of sunspot (left) splits absorption line according to Zeeman effect (right). Credit: In public domain {{PD-US}}. https://upload.wikimedia. org/wikipedia/commons/9/9e/ Sunzeeman1919.png.*

2. Nuclear magnetic resonance (NMR)

The phenomenon of nuclear magnetic resonance (NMR)[7] is the physical absorption and re-emission of electromagnetic radiation, which occurs at a characteristic and specific resonance frequency (typically, 40–1000 MHz, and thus in the radiofrequency range), as is a property of the magnetic nature of a particular atomic nucleus, and the intensity of the applied magnetic field. It is a feature of all nuclei that contain an *odd* number of protons and/or neutrons to possess an intrinsic magnetic moment and angular momentum, [*i.e.* the total spin (I) is non-zero]; in contrast, all nuclei with *even* numbers of both protons and neutrons have an overall spin, $I = 0$. The most frequently measured nuclei are ^1H and ^{13}C, although NMR has been observed from those of very many other elements too, including: ^2H, ^3H, ^6Li, ^{10}B, ^{11}B, ^{14}N, ^{15}N, ^{17}O, ^{19}F, ^{23}Na, ^{29}Si, ^{31}P, ^{35}Cl, ^{113}Cd, ^{129}Xe, and ^{195}Pt.

The NMR method can be augmented with ancillary techniques, such as *hyperpolarisation*[14] (polarisation of nuclear spins in a material far beyond thermal equilibrium conditions), and two-dimensional, three-dimensional and higher-dimensional multi-frequency experiments. Two essential steps are involved in achieving NMR: (1) The magnetic nuclear spins are first aligned (polarised) in an applied external magnetic field (B_0); and (2) the nuclear spin alignment is perturbed by the application of an electro-magnetic (radiofrequency) field: in modern NMR spectrometers usually in the form of an (RF) pulse. The precise perturbation frequency required for step (2) is determined both by the particular kind of magnetic nucleus being observed, and the strength of the applied magnetic field. The experimental arrangement is normally such that the two fields are mutually perpendicular, so to maximise the intensity of the NMR signal. It is the resultant response from the collective magnetisation (M) of the nuclear spins in a sample that is measured in NMR spectroscopy and magnetic resonance imaging (MRI) experiments. By employing very strong (and very stable) applied magnetic fields

(B_0), a high spectral resolution is enabled for the precise measurement of chemical shifts, the Zeeman effect, and Knight shifts (as occur in metallic samples).

2.1 The ¹H NMR experiment

The following description for protons applies to any spin $I = \frac{1}{2}$ nucleus. A proton (¹H), has a spin of *one half* ($\frac{1}{2}$); the nuclear spin being designated as $I = \frac{1}{2}$, with quantum numbers (labels) $m_I = +\frac{1}{2}, -\frac{1}{2}$. In the absence of an external magnetic field, protons with spin $+\frac{1}{2}$ or $-\frac{1}{2}$ have the same energy; however, as the field (B_0) is applied, those $+\frac{1}{2}$ are lowered, and those $-\frac{1}{2}$ are raised in energy, relative to the zero field situation (Figure 2). This may be represented by Eqn (1), where E_0 is the energy of both $m_I = +\frac{1}{2}$ or $-\frac{1}{2}$ states before the magnetic field is applied. (One can imagine the spinning proton [hydrogen nucleus] behaving as a tiny magnet, which senses the influence of the far stronger external magnetic field.) As an additional factor, an excess population of $m_I = +\frac{1}{2}$ appears, due to the Boltzmann distribution of proton spins between this state and the $m_I = -\frac{1}{2}$ state, at higher energy.

$$Em_I = E_0 - g_N\mu_N B_0(1-\sigma)m_I \tag{1}$$

There is, therefore, an energy level *splitting* introduced between the $m_I = +\frac{1}{2}$ and $m_I = -\frac{1}{2}$ states, as it is described by Eqn (2), and which is seen to increase in direct proportion to the strength of the external magnetic field (B_0):

$$\Delta E = g_N\mu_N B_0(1-\sigma) \tag{2}$$

$$\Delta E = \gamma_N(h/2\pi)B_0(1-\sigma). \tag{3}$$

In [Eqns (1) and (2)], g_N and μ_N are constants (respectively the 'nuclear g-factor' and the 'nuclear magneton') which determine the intrinsic magnetic field strength of a given spinning nucleus, while σ (the 'shielding constant') determines the strength of the magnetic interaction between the external magnetic field (B_0) and the nucleus (proton). Since $\gamma_N = g_N\mu_N(2\pi/h)$, the energy level splitting can also be expressed by Eqn (3), where γ_N is the gyromagnetic ratio for the nucleus, and h is Planck's constant. Resonant absorption by nuclear spins will occur only when electromagnetic radiation is applied to the sample (as contained in an applied magnetic field) which matches the energy difference (ΔE) between the $+\frac{1}{2}$ and $-\frac{1}{2}$ nuclear spin energy levels. This radiation corresponds to the angular (Larmor) precession frequency, ω. [As measured in Hz (*i.e.* $v = \omega/2\pi$), $v = -(\gamma_N/2\pi)B_0$, which amounts to 42.57748 MHz T⁻¹ for ¹H)]. For magnetic fields up to roughly 20 T, such NMR frequencies typically correspond to the radiofrequency (RF) range of the electromagnetic spectrum; σ-values are not normally determined directly, but 'chemical shifts' are generally labelled δ, and quoted relative to a standard material (*e.g.* TMS, Me$_4$Si) in parts-per-million (ppm) of the external magnetic field strength. Either way, σ or δ, the shielding constant/chemical shift represents the local electronic environment of the proton, which resonates diagnostically at different magnetic field values, according to the kind of chemical functional group that it occupies[7,15,16]. A particular advantage of
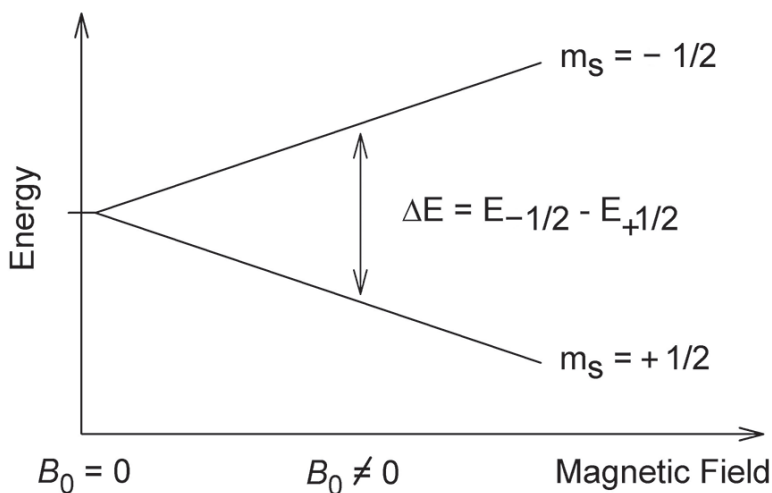
Christopher J. Rhodes

Figure 2 *Splitting of nuclear spin energy levels by an external magnetic field (B) in an ¹H NMR experiment. Credit: JBancroftBrown. https://upload.wikimedia.org/wikipedia/commons/6/67/NMR_splitting.gif.*

working at higher magnetic fields is that a far better resolution of different chemical shifts is obtained, which may aid in the interpretation of NMR spectra from complex molecules.

2.2 Methods of NMR spectroscopy

2.2.1 Continuous wave (CW) NMR spectroscopy

While it is, in principle, possible to obtain NMR using an instrument which varies the frequency of the RF radiation, while keeping the applied magnetic field strength constant, in practice, it is more usual to employ a source of fixed frequency (continuous wave) and to vary the current in an electromagnet, which allows the magnetic field strength to be 'scanned' over a chosen range. The original NMR spectrometers worked in this way, as remained the case for the first two decades or so, following their commercial production in the early 1960s. Such CW instruments were relatively cheap to operate and maintain, many of which operated at a 60 MHz frequency (as a 16 year old school-leaver, I first worked on a [Varian A-60] 60 MHz NMR in the 1970s, at Beecham Pharmaceuticals) with electromagnets (1.4 T) cooled by water flowing through them. 90 MHz and finally 100 MHz CW instruments later became available, but this 'brick wall' of frequency was only broken through with the advent of far more powerful superconducting magnets[16], which are cooled with liquid helium; hence, the frequency climbed steadily with improved magnet technology, up to the current world record, which stands at 1,020 MHz[17]. Since CW spectroscopy probes the NMR response at successive individual resonances, it lacks the efficiency provided by Fourier analysis methods (Section 2.2.2), and the

signal-to-noise ratio tends to be poor. Signal averaging methods, where the spectra from repeated scans are simply added together, can partially improve the situation, because the positions of the NMR signals do not change from one scan to another, and so the signals add linearly. In contrast, the random noise adds as the square root of the number of spectra, and so the signal-to-noise ratio also increases in proportion to the square-root of the number of spectra measured (*i.e.* if 100 spectra are summed, the cumulative signal increases by a factor of 100, but the noise as 10. Hence the enhancement in signal-to-noise is $100/10 = 10$).

2.2.2 Fourier-transform NMR spectroscopy (FT NMR)

Pioneering efforts to improve beyond the basic CW approach involved irradiating the sample simultaneously with a number of different radiofrequencies; however, it is now usual to measure the entire NMR signal intensity following the application of short pulses of 'carrier' frequency RF radiation. The carrier encompasses a range of frequencies, centred about the fundamental carrier frequency, and the bandwidth (excitation range) is inversely proportional to the duration of the pulse. Hence, the Fourier transform of a short pulse contains contributions from all the frequencies in the region of the centre-frequency. When the pulse is applied, all the single-quantum NMR transitions from a collection of nuclear spins are excited simultaneously. From an instrumental standpoint, this accords with a tilting of the magnetisation vector (M_0) away from its original alignment with the (z) axis of the external magnetic field (B_0) – the equilibrium position – into the x,y plane. Having been disturbed from equilibrium, the magnetisation vector precesses about the external magnetic
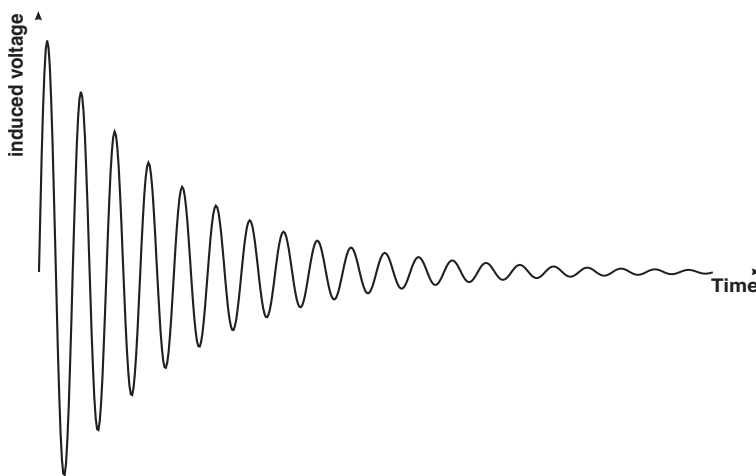

Figure 3 *NMR free-induction decay (FID) signal. The duration of the NMR signal is ultimately limited by* T_2 *relaxation, but mutual interference of the different NMR frequencies present also causes the signal to be damped more quickly. When NMR frequencies are well-resolved, as is typically the case in the NMR of samples in solution, the overall decay of the FID is relaxation-limited and the FID is approximately exponential (with the time constant* T_2 *changed, indicated by* T_2^**). Credit: GyroMagician.* https://upload.wikimedia. org/wikipedia/commons/1/1e/Nmr_fid_good_shim_EN.svg.

Christopher J. Rhodes

field axis at the NMR transition frequency, which induces an oscillating current in a receiver coil, and generates an electrical signal known as the free induction decay (FID) (Figure 3). This is a time-domain (intensity *vs* time) signal and contains the vector sum of the NMR transitions from all the excited nuclear spins; it may be converted to the frequency-domain (intensity *vs* frequency) NMR spectrum by Fourier transformation.

2.2.3 Multi-dimensional NMR Spectroscopy

Multi-dimensional NMR spectroscopy is a version of FT NMR which employs a sequence of (at least two) pulses and variable time periods. Thus, in three dimensions, there is a variation of two time sequences, and in four dimensions, three are varied. Of the many different kinds of experiment that arise from this approach, it is possible to detect the kinds of nucleus–nucleus interactions that enable the magnetisation transfer to occur. These are generally classified as being *through-bond* interactions and *through-space* interactions: the latter arising *via* the nuclear Overhauser effect, which may be exploited to determine interatomic distances, *e.g.* for molecules in solution using 2D-FT NMR. In 1971, Jean Jeener, a Professor at Université Libre de Bruxelles, first proposed the COSY experiment, which was later actually performed by Walter P. Aue, Enrico Bartholdi and Richard R. Ernst, who published[18] their results in 1976. It was Ernst who was primarily responsible for the development of multi-dimensional FT NMR, and 2D-FT NMR of small molecules in particular, winning the 1991 Nobel Prize in Chemistry[19] for his contributions to the development of the methodology of high resolution NMR spectroscopy. Structural determinations of biopolymers such as proteins and even small nucleic acids in solution can be made using multi-dimensional NMR techniques. Along with John Bennett Fenn and Koichi Tanaka, Kurt Wüthrich was awarded the 2002 Nobel Prize in Chemistry[20] for his development of NMR spectroscopy for determining the three-dimensional structure of biological macromolecules in solution.

One of several types of two-dimensional nuclear magnetic resonance (2D-NMR) is 'correlation spectroscopy' (more commonly referred to as COSY), which forms a family, along with *J*-spectroscopy, exchange spectroscopy (EXSY), nuclear Overhauser effect spectroscopy (NOESY), total correlation spectroscopy (TOCSY) and heteronuclear correlation measurements, such as HSQC, HMQC, and HMBC. In correlation spectroscopy, the emission is focussed upon the peak of an individual nucleus, and if its magnetic field is correlated with another nucleus by through-bond or through-space coupling, a spectroscopic response can be further detected at the frequency of the correlated nucleus. This allows information to be obtained about the structures of molecules that are too complex to investigate by means of one-dimensional NMR.

2.2.4 Solid-state NMR spectroscopy/magic angle spinning (MAS)

For a variety of reasons, it is not always possible to study molecules in solution, either using NMR or other methods, and hence solid samples must be investigated. However, NMR measurements of solid media such as crystals, microcrystalline

powders, gels, and anisotropic solutions, are dominated by the anisotropic nucleus–nucleus dipolar couplings and the anisotropy in the chemical shift tensors. These interactions are typically averaged to zero, by rapid molecular tumbling, in solution-phase NMR experiments, although they may contribute to a broadening of the isotropically-centred spectral lines. However, certainly in the case of ^{13}C nuclei, spectra can be obtained which are of comparable resolution to those measured in liquid solutions, when special techniques are employed to average-out the anisotropic nuclear magnetic interactions. In the method known as magic angle spinning (MAS)[21], the sample is spun rapidly (at a rate of 1–100 kHz) around an axis which subtends the so-called 'magic angle' θ_m (which is ~54.74°) with respect to the (z) direction of the static magnetic field B_0, and for which $\cos^2\theta_m = \frac{1}{3}$ (Figure 4). This has the effect of averaging the anisotropic (orientation-dependent) magnetic interactions, and it is at the magic angle that the ('through-space') nucleus–nucleus magnetic dipole–dipole interactions, and chemical shift anisotropies, average to zero, since here the relevant anisotropic function vanishes, $i.e.$ $3\cos^2\theta_m - 1 = 0$. Thus, the orientational averaging that occurs through molecular tumbling in a liquid, is emulated by MAS of a solid sample, causing a narrowing of the signal and permitting a determination of the isotropic spin–spin coupling and chemical shift values. There is a variety of applications in which solid-state NMR may be beneficially used, $e.g.$ in structure investigations of membrane proteins and protein fibrils, and indeed many types of different polymers, and in the analysis of inorganic materials.
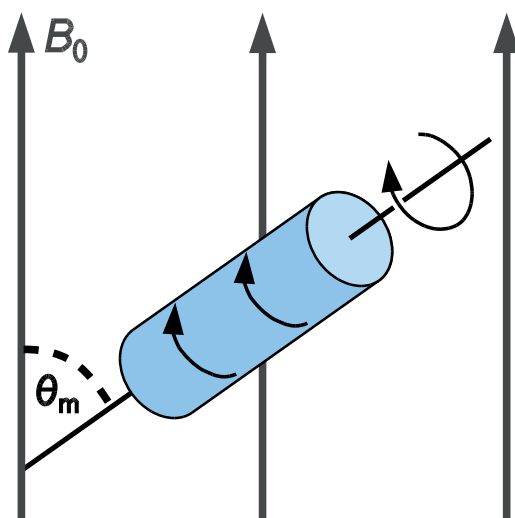

Figure 4 Magic-angle-spinning (MAS) NMR experiment. The sample (blue) is rotating at a high frequency (up to ca 100 kHz) within the applied magnetic field (B$_0$). It is tilted by the magic angle (θ_m ~54.74°) with respect to the direction of the magnetic field orientation. Credit: Dtrx. https://upload.wikimedia.org/wikipedia/commons/a/ab/MagicAngleSpinning.svg.

2.3 Molecular structural information that may be obtained from NMR

2.3.1 Chemical shift

As we have seen in Section 2.1, the energy difference between the two (proton) spin states of spin $I = \frac{1}{2}$ nuclei induced by a magnetic field of given strength is proportional to the intrinsic magnetic properties of the particular nucleus (nuclear magneton, g_N, and nuclear g-factor, μ_N). However, despite the fact that these constants must be the same for all protons, protons from different functional groups in molecules do not all resonate at the same frequency, as a consequence of the differing electronic environments of the nuclei (*e.g.* –CH_3 *cf.* –CH_2–). The electrons in molecules respond to the influence of the far stronger external magnetic field, and in so doing, produce smaller local magnetic fields that act in opposition to it. It can thus be said that the local fields 'shield' the protons from the external magnetic field, so that in order to achieve resonance, the latter must be increased to further separate the energy levels, to match the energy of the applied RF radiation, which can then be absorbed by the sample. These 'adjustments' to the effective field experienced by a proton are of the order of parts per million (ppm) of the applied magnetic field, and for example, the peak from an aldehyde (CHO) group is shifted (to low-field) by about 10 ppm from the resonance of the protons in the TMS reference sample, since the C=O group withdraws electron density from the vicinity of the unique CHO proton and deshields it, so that it resonates at a smaller external magnetic field strength if the magnetic field is being scanned, (or resonates at a higher frequency, if the field is kept constant). By quoting chemical shifts relative to a reference signal (usually TMS, Me_4Si), issues of the dependence of the absolute signal position (in field or frequency units) on external magnetic field strength and the reference frequency are circumvented. If the NMR resonance frequencies are divided by the spectrometer frequency (*i.e.* dividing Hz by MHz), the ratios are relatively small and so it is convenient to multiply them by a factor of one million: thus, a range of 'chemical shift' values is obtained, in units of parts per million (ppm)[7,16]. Proton chemical shifts are a result mainly of local electron densities, and can therefore be predicted with reasonable accuracy; however, for the nuclei of many heavier elements, other factors including the contribution from excited states ('paramagnetic' contributions to shielding tensors) are major determinants of chemical shift values, and are more difficult to estimate in advance.

The observation of different chemical shifts provides information about the structure of molecules, and some prediction can be made of the kind of NMR spectrum that a given chemical compound would give. Thus we would expect the ^1H NMR spectrum of ethanol (CH_3CH_2OH) to reveal three distinct chemical shifts, from the CH_3 group, the CH_2 group and the OH group. In regard to their anticipated positions, we can say that typically a CH_3 group resonates at *ca* 1 ppm, while a CH_2 attached to an (electron withdrawing) OH group would resonate in the region of 4 ppm. The OH resonance position is somewhat more viable, due to a combination of the electron withdrawing effect of the O-atom (partially offset by

the lone pair electrons on the O-atom which shield the OH proton), and the degree of H-bonding, which is solvent-dependent: thus, we might expect a chemical shift to occur anywhere within the range of 2–6 ppm. It might further be expected that the relative heights of the resonance signals from the ^{1}H NMR spectrum of ethanol would reflect the number of protons in each functional group (*i.e.* a ratio of 3:2:1, from CH_3CH_2OH); however, different signals have different linewidths and so it is necessary to determine the area under each signal, which is done using an instrumental procedure called 'integration'. Indeed, for very simple one-dimensional NMR spectra, this works fairly well and an appropriate proportionality is obtained between the integrated signal intensities and the number of protons in each functional group. In contrast, for more complex experiments, *e.g.* those used to obtain ^{13}C NMR spectra, the integrated signal areas depend on the relaxation times/rates (Section 5) of the nucleus in its particular environment, and also its scalar and dipolar coupling constants. Thus, as a general rule, the intensities of signals in ^{13}C NMR spectra are not considered as reliable for analytical (structure elucidation) purposes. As noted in Section 2.1, it is possible to increase the resolution of different chemical shifts by working at higher magnetic field strengths, which may aid in the interpretation of complex NMR spectra containing multiple, overlapping resonances.

2.3.2 Spin–spin coupling between magnetic nuclei

In terms of elucidating molecular structures from one-dimensional NMR spectra, the phenomenon of spin–spin coupling (also called *J*-coupling, or scalar coupling) between NMR active nuclei can provide important information. This coupling arises from the polarisation of the spins of electrons in chemical bonds between magnetically active nuclei by the nuclear spins, and can be measured from the splitting patterns of fundamental NMR resonance signals, located at particular chemical shift positions. Coupling of this kind enables details of the connectivity of atoms in a molecule to be determined. For spin $I = \frac{1}{2}$ nuclei, the '$n + 1$ rule' applies, (*i.e.* coupling of a given nucleus to n equivalent spin $I = \frac{1}{2}$ nuclei gives $n + 1$ lines), and the intensity ratios that arise in the resulting multiplet splitting patterns may be determined using Pascal's triangle (Figure 5). Additional splittings of each component of the multiplet are induced by coupling to further nuclei, and as an example, we see that coupling of a nucleus to two different spin $I = \frac{1}{2}$ nuclei with significantly different coupling constants gives rise to a *doublet of doublets* pattern. In the ^{1}H NMR spectrum of ethanol (Figure 6), the resonance from the CH_3 group is split into a *triplet* with an intensity ratio of 1:2:1 by the two neighbouring CH_2 protons, while the resonance from the CH_2 is split into a *quartet* with an intensity ratio of 1:3:3:1 by the three neighbouring CH_3 protons. It might be expected that the CH_2 proton resonance would display a further *doublet* splitting – giving an overall *doublet of quartets* pattern – from the hydroxyl proton, but in practice, the rapid exchange of hydroxyl protons between molecules means that this coupling is not detected. While this general description applies to other $I = \frac{1}{2}$ nuclei, *e.g.* ^{31}P, ^{19}F, when nuclei with spin greater than $\frac{1}{2}$ are present, it is not possible to use the simple Pascal's triangle to

¹H	Intensity Ratio
1	1:1
2	1:2:1
3	1:3:3:1
4	1:4:6:4:1
5	1:5:10:10:5:1
6	1:6:15:20:15:6:1

Figure 5 Pascal's triangle, showing relative intensity of lines in multiplet patterns arising from coupling to groups of n *equivalent spin* I = ½ *nuclei, e.g. protons.*
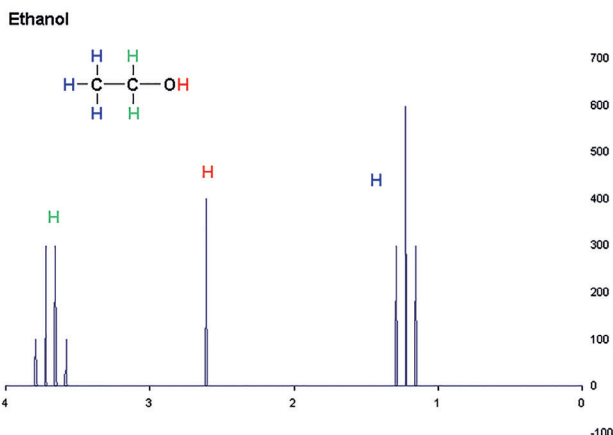

Figure 6 ¹H NMR spectrum of ethanol (100 MHz in CDCl₃) plotted as signal intensity vs chemical shift. There are three different types of H-atoms in ethanol regarding NMR. The proton on the –OH group is not coupling with the protons from the other H atoms and appears as a singlet, but the protons from the CH₃– and the –CH₂– groups are spin-coupled, resulting in a triplet and quartet respectively. Credit: T.vanschaik. https://upload. wikimedia.org/wikipedia/commons/f/f2/1H_NMR_Ethanol_Coupling_shown.GIF.

determine the multiplicities and line intensities that arise from coupling to them. This is because there is now a greater range of spin quantum numbers than the simple pair of $+\frac{1}{2}, -\frac{1}{2}$ options, *i.e.* coupling to deuterium (spin $I = 1$) nucleus results in a *1:1:1 triplet* splitting pattern because there are three possible spin states (+1, 0, –1), while a spin $I = \frac{3}{2}$ nucleus will in principle result in a *1:1:1:1 quartet* splitting from the four possible spin states $(+\frac{3}{2}, +\frac{1}{2}, -\frac{1}{2}, -\frac{3}{2})$. Thus, in combination with chemical shift information, both the particular chemical environment (functional group) of the nuclei and the number of magnetically active nuclei in the neighbourhood of particular nuclei can be determined.

2.3.3 Second-order NMR spectra

So long as the coupling constant (in Hz) is small in comparison with the difference in chemical shifts between magnetically inequivalent nuclei (both expressed in

frequency units), the above description holds. However, when the ratio of coupling constant to chemical shift difference decreases (*i.e.* the coupling constant increases or the chemical shifts get closer together), initial distortions in the multiplet peak intensities are observed, but as the ratio becomes smaller still, more complicated patterns emerge which are not so straightforward to analyse. The complexity is greater when more than two coupled spins are involved, and it is found that some of the peaks increase in intensity while others are reduced: in some cases, the reduction in intensity of some of the multiplet peaks is sufficiently great that they are masked by the background noise, although the total integrated area of the multiplet remains the same. However, in many examples, the distortions are manifested as a sequential levelling-down of the peaks (loss of intensity from left-to-right or from right-to-left) in multiplets from spin-coupled functional groups ('*roof effects*'), and this can help to identify the manner of chemical bonding between them: it is sometimes said that the inclines of these related roofs 'point to one another'. Since it is the ratio of (coupling constant frequency)/(frequency difference between chemical shifts of coupled groups) which determines these second-order effects, they are observed less commonly (or in smaller degree) at the far higher magnetic fields employed in modern NMR spectrometers (which cause a greater separation of chemical shifts), than was the case with the earlier, *e.g.* 60 MHz, instruments.

2.3.4 Spin-decoupling

Spin-decoupling involves the irradiation of a sample at a specific frequency or frequency range, in order to remove the effects of coupling between chosen nuclei. This may either simplify the appearance of NMR spectra, or provide further structural information about a complex molecule, *e.g.* showing which nuclei are coupled together. If the nuclei that are being irradiated, and the nuclei being observed are of the same isotope, the technique is referred to as *homonuclear decoupling*; if, however, the two groups of nuclei are from different isotopes, the term *heteronuclear decoupling* is used. It is possible to irradiate at frequencies for all nuclei of a particular isotope (broad-band decoupling), or a select range of frequencies (even one) can be used.

If a ^{13}C spectrum is run in the absence of proton-decoupling, each of the ^{13}C signals is split into a pattern which reflects the number of H atoms that each carbon atom is coupled to, and while being useful in principle, it adds complexity to the spectral patterns. To remove this effect, and provide simplification, ^{13}C NMR spectra are usually run in the *fully proton decoupled* mode, where the sample is irradiated at a broad band of ^{1}H frequencies, to decouple all ^{1}H from all ^{13}C nuclei in the sample. Thus, signals in fully proton decoupled ^{13}C spectra in the majority of organic compounds contain only single peaks (Figure 7), meaning that the number of equivalent sets of carbon atoms in a molecule can be determined simply by counting the number of peaks. As an additional advantage, removing all proton couplings in this way tends also to provide an increase in the intensity of the ^{13}C signals. [^{13}C NMR is inherently far less sensitive than ^{1}H NMR: on the basis of the ratio
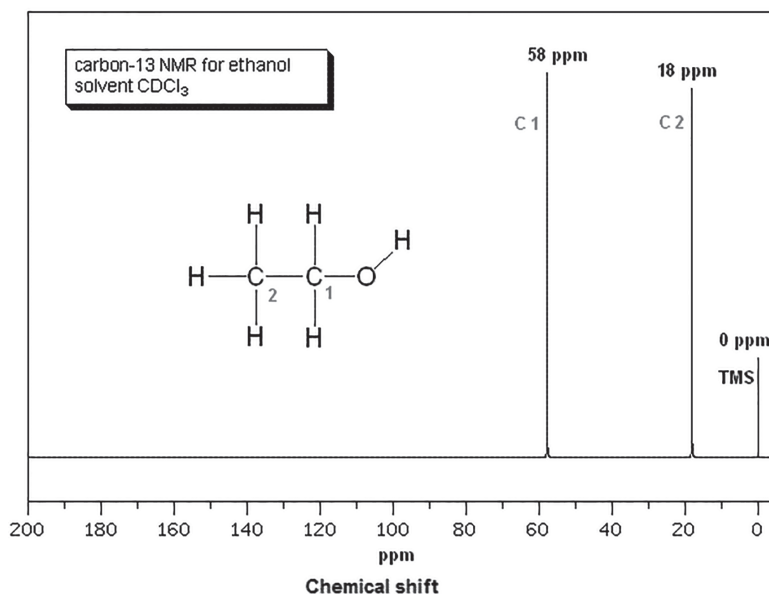
Figure 7 Fully proton-decoupled ^{13}C NMR spectrum of ethanol (25 MHz in CDCl₃) showing just a single peak for each carbon atom in the molecule. Credit: Chris Evans. https:// upload.wikimedia.org/wikipedia/commons/d/d8/13C_NMR_ethanol.GIF.

of gyromagnetic ratios cubed ($\gamma^{13}_{C}/\gamma^{1}_{H}$)³, we may deduce that ^{13}C has a sensitivity only 1.589% that of ^1H. However, the much lower natural abundance of ^{13}C (1.1%), compared with ^1H (99.985%), means that the actual sensitivity of ^{13}C NMR is just 0.0175% (1/5720) that of ^1H NMR.]

By means of *off-resonance decoupling* of ^1H in ^{13}C NMR spectroscopy, only ^1H atoms directly bonded to a particular carbon atom will give rise to splitting in its ^{13}C resonance. Thus, CH_3 groups would appear as quartets, CH_2 groups as triplets, CH groups as doublets, and quaternary carbon atoms as singlets. In *specific proton decoupling* (also called band-selective or narrow-band decoupling), a specific 'narrow' ^1H frequency band is used, often in order to determine the connectivities between nuclei in molecules. Thus, if a single ^1H signal is irradiated (at its resonance frequency), this will cause a collapse of the spin (J) coupling pattern in only those other signals from ^1H nuclei which are J coupled to the ^1H nucleus whose signal is being irradiated. Since the remainder of the spectrum is unaffected, this technique of specific decoupling is very useful for assigning signals to particular atoms/functional groups in molecules, and aiding an overall determination of molecular structures.

3. Biomolecular NMR spectroscopy

3.1 Proteins

The use of NMR spectroscopy to obtain high resolution three-dimensional structures of proteins[22], has emerged as a method in structural biology, and which is

complementary to X-ray crystallography. NMR spectroscopy is generally used on proteins with a molecular mass of less than 35 kDa, although there are exceptions to this, and it is almost the only method for the study of proteins that innately lack regular structure. Conformation-activity relationships may be determined using NMR methods, to determine changes in the protein structure caused by its interaction with a potential drug molecule, and to relate this to the known biochemical activity of the latter. Even though protein molecules are larger (often by several orders of magnitude) than the small organic molecules that NMR is more commonly used to investigate, the fundamental theoretical principles remain valid. However, simple one-dimensional NMR spectra of proteins present so many overlapping signals that it is not possible to analyse them as is done for smaller molecules, and there are limitations in using natural proteins, due to the fact that the principal carbon isotope, ^{12}C, is magnetically inactive and it is difficult to obtain high resolution data from the naturally occurring nitrogen isotope, ^{14}N, as a result of its nuclear quadrupole moment. Instead, more sophisticated, multidimensional (2, 3 or 4D) measurements are employed, and on proteins that have been enriched in isotopes such as ^{13}C and ^{15}N, to increase NMR sensitivity. Experiments based on the nuclear Overhauser effect (NOE) are particularly important for determining distances between pairs of atoms within the particular protein molecule, and these parameters may then be used to generate a three-dimensional structure of the molecule. It is also possible to use NMR as a means for determining the molecular dynamics and conformational flexibility of different regions and segments of a protein.

3.2 Nucleic acids

Advances in NMR, as a means to determine structural and dynamical information for nucleic acids, such as DNA and RNA, have been sufficiently spectacular that by 2003, practically half of all known RNA structures had been determined using its methods[23]. Although there are similarities between the study of proteins and nucleic acids using NMR methods, there are also significant differences, due to the differing nature of the molecules involved. In particular, nucleic acids contain a smaller proportion of hydrogen atoms than do proteins, and the nucleic acid double helices are inflexible and directional, which prevents them from 'folding back' on themselves such that 'long-range' correlations are obtained[24]. 2D-NMR methods such as COSY and total coherence transfer spectroscopy (TOCSY), are almost always used for the study of nucleic acids, to determine through-bond nuclear spin–spin couplings, and NOESY, to determine interactions between nuclei that are in close spatial proximity[25].

From such parameters as coupling constants and NOESY cross-peaks, information can be obtained pertaining to *local* structure, *e.g.* bond angles in glycosides, dihedral angles (*via* the Karplus equation[16]), and the conformations of sugar units. By combining such local structural parameters with molecular modelling and other calculations, it is possible to develop a larger-scale picture of the nucleic acid molecule. Such non-standard geometries as bent helices, non-Watson–Crick

base pairing, and coaxial stacking can also be determined using NMR methods, and it has proved possible to investigate the structure of natural RNA oligonucleotides, which tend to adopt complex arrangements such as stem-loops and pseudoknots. The binding between nucleic acids and other molecules, such as those of drugs and proteins, can be probed on the basis of shifts in resonances that take place when another molecule binds to them[25].

3.3 In vivo *magnetic resonance spectroscopy (MRS)*

In vivo magnetic resonance spectroscopy (MRS)[26] can be used in a complementary fashion with the better known magnetic resonance imaging (MRI) (Section 4) to characterise tissue in living animals. Both methods employ ^{1}H NMR phenomena, which in MRI are transformed into spatial images of the brain, and in MRS, the concentrations of critical brain metabolites are determined[27]. Accordingly, metabolic changes associated with tumours (brain, breast and prostate), epilepsy, strokes, seizure disorders, Alzheimer's disease, Parkinson's disease, Huntington's chorea, pituitary tuberculosis[28], depression and other mental diseases of the brain have all been studied using MRS. In MRI, it is the ^{1}H NMR resonances from H_2O that are measured, while MRS can be used to determine other molecules that are associated with various disease conditions by comparing observed *in vivo* signals with known 'fingerprint' spectra. The frequencies of MRS equipment can be varied to measure resonances from ^{1}H, ^{31}P, ^{13}C, [23]Na and ^{19}F, in order to detect particular metabolites. Formerly, MRS equipment lacked sufficient sensitivity for *in vivo* work, but more recent developments in RF-coil technology and the use of stronger external magnetic fields have brought the method into quasi-clinical use. As an example of this, we may note that, it has been shown that in combination with MRI, a 3D MRS measurement can determine the presence of a malignant degeneration of prostate tissue with an accuracy of around 90%. It is likely that a concerted application of MTI and MRS may provide useful information in planning both biopsy and therapy procedures for the prostate, and furthermore be able to monitor the effectiveness of treatments for prostate cancer[29].

3.3.1 Applications of MRS

As we have seen, the ^{1}H NMR spectra from specific functional groups are characterised by particular chemical shifts, and so, specific metabolite compounds can be identified according to unique patterns of their ^{1}H NMR resonances, previously 'fingerprinted' from known compounds. Of the metabolites that have been so identified from their MRS spectra, we may include the following[30]:

- *N-acetyl aspartate (NAA)*: main peak at 2.02 ppm. While its presence in normal conditions indicates neuronal and axonal integrity, reduced levels of NAA indicate loss of, or damage to neuronal tissue, as can be caused by many different kinds of brain injury.
- *Choline*: main peak at 3.2 ppm. Increased levels of choline indicate an increase in cell production or membrane breakdown, as can be a result of demyelination or the presence of malignant tumours.

- *Creatine and phosphocreatine*: main peak at 3.0 ppm. Since creatine is a marker of metabolic energy processes in the brain, a gradual reduction in creatine levels, along with other major metabolites, indicates tissue death or major cell death, as caused by disease, injury or an insufficient blood supply. In contrast, elevated concentrations of creatine might be a consequence of cranialcerebral trauma.
- *Lipids*: main peaks in the 0.9–1.5 ppm region. An increase in brain lipids provides a further indication of necrosis. However, since lipids are also present in biological tissue such as the fat in the scalp, and in the area between the scalp and skull, false indications are possible from the MRS spectra.
- *Lactate*: shows a doublet resonance at 1.33 ppm. Since the concentration of lactate is normally below the detection limit of MRS, it is not visible, but when it is observed, the presence of glycolysis is indicated, as has been initiated in an oxygen-deficient environment. There are a number of possible reasons for this, such as ischemia, hypoxia, mitochondrial disorders, and some types of tumour.
- *Myo-inositol*: main peak at 3.56 ppm. Increased concentrations of myo-inositol have been detected in patients with Alzheimer's disease, dementia, and HIV.
- *Glutamate and glutamine*: characterised by a series of resonances between 2.2 and 2.4 ppm. As used in combination with MRI (or other imaging technique), MRS can be used to detect changes in, or significantly abnormal, concentrations of glutamate and glutamine. Hyperammonemia and hepatic encephalopathy are two possible conditions that may give rise to elevated levels of these metabolites.

MRS may be used in combination with MRI (Section 4). Figure 8 shows an MRI brain scan (taken in the 'axial plane', *i.e.* slicing in the front-to-back/side-to-side direction through the head) which reveals a brain tumour (meningioma) at the bottom right of the image. The red box identifies the volume (a cube with 2 cm sides which produces a square when intersecting the 5 mm thick slice of the MRI scan) of the brain to which MRS was applied. As noted, signals from particular metabolites appear at characteristic chemical shifts (Figure 9), and that highlighted in red (CH_3
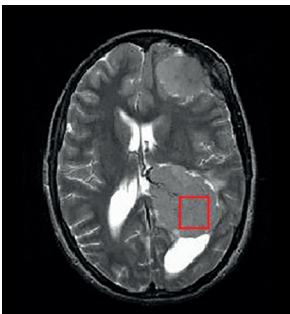

Figure 8 MRI brain scan showing a brain tumour at the bottom right of the image. Credit: Dj manton at English Wikipedia. https://upload.wikimedia.org/wikipedia/commons/f/f5/MRS_localiser_image.jpg.
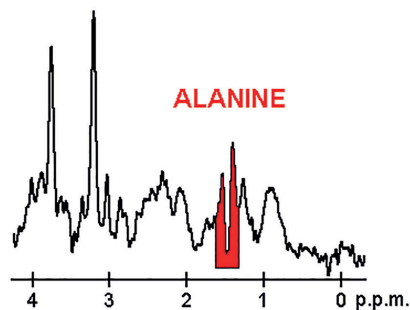
Figure 9 MRS of brain tumour region (Figure 8), showing the presence of the amino-acid, alanine. Credit: Dj manton at English Wikipedia. https://upload.wikimedia.org/wikipedia/commons/a/a0/MRS_spectrum.gif.

resonance centred at 1.4 ppm, split into a doublet from the CH_3CH proton) reveals the presence of the amino acid alanine ($CH_3CH(NH_2)CO_2H$. Other major metabolites are choline (3.2 ppm) and creatine (3.0 ppm).

3.4 Functional magnetic resonance spectroscopy of the brain (fMRS)

Functional magnetic resonance spectroscopy of the brain (fMRS)[31] uses MRI to study the metabolism of the brain during a period when the brain is activated by some stimulus. However, fMRS usually shows spectra of resonances, whose relative areas provide a measure of the relative concentrations of metabolites. In contrast with MRS (which records spectra from single metabolites), fMRS records different spectra simultaneously from which to determine the relative concentration dynamics of different metabolites during particular types of brain function. A relatively new version of fMRS is termed *functional diffusion-weighted spectroscopy* (fDWS), which monitors the diffusion of brain metabolites caused by activation of the brain[32]. While *in vivo* MRS is now applied extensively for clinical use, fMRS is, as yet, mainly used to undertake fundamental clinical research, *e.g.* to study the dynamics of metabolites in patients suffering from epilepsy, migraine and dyslexia, and also to study the function of healthy brains. A major aim of research into fMRS is to obtain a detailed understanding of metabolic processes for the use of energy in the brain, and to improve and ensure the reliability of fMRS methods; metabolic studies may be made in other parts of the body than the brain, such as the heart, and muscles in general. Since it is the more magnetically sensitive nucleus, most fMRS measurements are made on ^{1}H, to determine the concentrations of metabolites, and their dynamics; however, ^{13}C is better suited as a probe of the pathways and fluxes of brain metabolism, which is usually introduced to the patient *via* infusion or ingestion of ^{13}C-labelled compounds, to increase the concentration of this isotope to above its natural abundance (1%). ^{13}C fMRS is commonly termed *functional ^{13}C MRS* or simply *^{13}C MRS*. As a result of the complex spectral signatures from different metabolites and their relatively low concentrations, the signal-to-noise ratios tend to be low in MRS spectra of an actual, living brain, and so it is necessary to accumulate a number of spectra and average them. However, the spectral acquisition times should not be too long in duration, in order that an effective dynamic rate of change in metabolite concentration can be obtained. By using high magnetic fields, both signal-to-noise and separation of chemical shifts are enhanced, thus permitting the detection of a greater number of metabolites simultaneously, and providing more insight into the detailed metabolite concentration dynamics. Improvements in the instrumentation for fMRS are continually forthcoming, in the form of more powerful magnets and more effective techniques for data acquisition: collectively thus providing increased spectral and temporal resolution. It is possible to detect probably 18 different metabolites using a 7 T instrument, while temporal resolution is now at around 5 s[33] as compared with about 7 min in the early fMRS studies[34].

4. Magnetic resonance imaging (MRI)

Since the resonance frequency of a particular nucleus is in direct proportion to the external magnetic field strength (Section 2.1), if a magnetic field, whose intensity is different in different spatial regions (field gradient), is applied to the sample, a spatial 'image' of the distribution of nuclei within it can be generated. Thus, this phenomenon may be used in MRI to form pictures of the internal anatomy of the body, and to monitor various physiological processes and disease conditions. It is estimated that there are some 25,000 MRI scanners in operation worldwide[35], and demand for the technology increases continually within the healthcare industry, leading to some degree of speculation regarding its cost effectiveness (since the technology is not cheap) and the risk of over-diagnosis[36]. MRI provides an alternative to using X-ray techniques, *e.g.* computed tomography (CT), and can be considered as a 'safer' option, in that it avoids the use of ionising radiation, although the use of X-rays in clinical applications is now well-controlled. MRI and CT can provide different kinds of information, and, as a generalisation, MRI is better suited for looking at soft tissue while CT is more useful for imaging more dense structures such as bones. In comparison with CT, MRI scans tend to take longer to run, and provide a noisier experience for the patient, who also has to be contained within the relatively narrow confines of the magnet, which can add a claustrophobic element. The presence of medical implants or other non-removable metal components may also be an issue in MRI as compared with CT, *e.g.* cochlear implants, cardiac pacemakers, shrapnel and metallic foreign bodies in the eyes. Resonances from ^{1}H nuclei (protons) of hydrogen atoms are generally used in MRI, as they exist abundantly in people and other living creatures mainly in their water and fat, and thus what MRI does primarily is to map-out where the water and fat are present in the body[37]. As is the case for FT NMR (Section 2.2.2), the nuclear spin energy transitions are excited using radiofrequency pulses, while the presence of magnetic field gradients allows a spatial determination of the amount of fat or water in the part of the body being scanned. It is possible to produce different contrast images between tissues (based on the relaxation times of the hydrogen atoms contained in them; Section 5), by adjusting the parameters employed in the pulse sequence. It is also possible to use MRI to obtain images of inanimate objects for various physical, chemical and engineering applications.

4.1 Medical applications of MRI

Since it offers improved resolution over CT scans, *e.g.* of the *posterior fossa*, MRI is the better method for imaging neurological cancers. The contrast that can be obtained between grey matter and white matter (Figure 10) using MRI also makes it highly suitable for the investigation of many ailments of the central nervous system, *e.g.* demyelinating diseases, dementia, cerebrovascular disease, infectious diseases and epilepsy[38]. Since the technique generates a collection of images at millisecond intervals, it is possible to study both functional and structural brain abnormalities in psychological disorders[39]. Cardiac MRI can be considered as being complementary

Figure 10 *'White matter' connections (tracts) in the brain obtained using diffusion MRI tractography. Credit: Gigandet et al. (2008) (see ref. 92).*

to other techniques, such as echocardiography, cardiac CT and nuclear medicine, and may be used to investigate myocardial ischemia and viability, cardiomyopathies, myocarditis, iron overload, vascular diseases and congenital heart disease[40]. MRI is of great assistance in the preoperative staging of rectal and prostate cancer, and may also provide useful information regarding the diagnosis, staging, and follow-up procedures for other types of tumours[41]. An MRI variant, called MR enterography, enables the investigation of inflammatory bowel disease and small bowel tumours to be made non-invasively, while MRI of the colon (MR colonoscopy) can assist in the detection of large polyps in patients with an increased risk of colorectal cancer[42]. It is also possible to image the spine, and to make assessments of diseases of the joints and of tumours in soft tissue.

5. Relaxation Times (T_1 and T_2)

In all forms of magnetic resonance, 'relaxation' is a term used to describe how signals *decay* with time, generally losing intensity or broadening[43]. The NMR signal arises from an excess population of an excited state (caused by an applied RF field/ pulse), and the process of relaxation is the restoration of an equilibrium population from this non-equilibrium condition. The decay of an NMR signal may be analysed in terms of two separate processes, each with their own time constants, referred to as *longitudinal* (along the axis of the external, applied magnetic field, *i.e.* the *z*-axis), *and transverse* (in respect to the *x,y*-plane, which is transverse, *i.e.* at right angles, to the applied magnetic field axis). The longitudinal relaxation time, T_1, causes the loss of signal intensity (*via* the return of spins from the excited state to the ground state), while the transverse relaxation time, T_2, causes the signal to broaden. In the absence of saturation, the width of the spectral line is determined entirely by T_2, which is accordingly also termed the *linewidth parameter*[44]. T_1 relaxation is the process by which the overall magnetisation of the sample (*M*) returns to its initial maximum value, with (M_0) longitudinal (parallel) to the axis of the applied magnetic field (B_0). This is a true process of energy emission/transfer, and in order for it to occur, it must be stimulated by the given nucleus experiencing a magnetic field which fluctuates (in the *x,y*-plane), at close to the Larmor frequency. The fluctuating field usually

arises from another proton or an electron, either in the same or in a close neighbour molecule, often as a result of a motional process, *e.g.* intramolecular motion (torsion about a chemical bond, conformational change), molecular reorientation and/or diffusion. The excess energy is transferred to the surrounding medium as heat, and as originally described for a solid (lattice), the term *spin-lattice relaxation time* is sometimes used to describe T_1. T_2 relaxation is the decay, or loss of phase-coherence of the components of magnetisation which are transverse (M_{xy}) to the applied magnetic field axis (M_z). (Thus, while T_1 can be thought of as an *enthalpy* change process, T_2 is one of *entropy* change. As a very simple analogy, we may consider a house [spin system] with a heater [excitation source] in one of the downstairs rooms. If the house is poorly insulated, the heat will readily escape through its external walls to the colder, outdoor regions [lattice], *i.e.* an overall loss of energy [T_1]. If, instead, the insulation is very good, so that the heat does not escape from the house, it instead spreads throughout its rooms, *i.e.* an internal energy distribution process [T_2].) Any process that perturbs either the number or relative positions of these transverse components will cause T_2 relaxation. Although any process that causes T_1 relaxation will also result in T_2 relaxation, it is possible for T_2 relaxation to occur alone. Isolated T_2 relaxation can be caused by dephasing, as a result of variations in static local fields, and 'flip-flop' exchanges (*e.g.* $-\frac{1}{2} + \frac{1}{2} \rightarrow +\frac{1}{2} -\frac{1}{2}$) between different spins. (If the spins all experience exactly the same magnetic field, they will all precess at the same rate and so keep their relative orientations; however, if they are all in slightly different local magnetic fields, the magnetic moments will precess at slightly different rates and eventually, the orientations become random[44]. Flip-flop exchanges will similarly ultimately randomise the orientations of the different spins.) Since the frequency of the fluctuating local magnetic field must be near to the (magnetic field dependent) Larmor frequency, in order to stimulate the longitudinal relaxation process, T_1 is much more sensitive to the external magnetic field strength than is T_2; typically[45], T_1 is longer than T_2, although there are exceptions to this. Measurements of T_1 and T_2 in all forms of magnetic resonance (NMR, MRI, EPR, μSR, and their variants) can be used to provide information about dynamic processes involving molecules, including (bio)chemical reactions, molecular reorientation and diffusion, and intramolecular processes, such as conformational changes. A measurement of relaxation parameters can also help to probe the internal environments of various kinds of materials, for physics and engineering applications, as well as those within the bodies of living creatures (Table 1).

6. Electron paramagnetic resonance (EPR)

6.1 Background and scope

Electron paramagnetic resonance (EPR)[8,15,46], also referred to as electron spin resonance (ESR), is a form of magnetic resonance spectroscopy which measures unpaired electrons specifically. It is, therefore, implicitly more restricted in its applications than is NMR[7], which in its various adaptations, measures a

Table 1 *Some approximate* T_1 *and* T_2 *values for proton nuclear spins in non-pathological human tissues[45], at an external magnetic field of 1.5 T*

Tissue type	Approximate T_1 value (ms)	Approximate T_2 value (ms)
Adipose tissues	240–250	60–80
Whole blood (deoxygenated)	1350	50
Whole blood (oxygenated)	1350	200
Cerebrospinal fluid (similar to pure water)	4200–4500	2100–2300
Gray matter of cerebrum	920	100
White matter of cerebrum	780	90
Liver	490	40
Kidneys	650	60–75
Muscles	860–900	50

comprehensive range of magnetic nuclei; but therein lies the advantage and subtlety of EPR. Unpaired electrons are created in a broad variety of samples which have often encountered fairly extreme conditions; *e.g.* high-energy (ionising) radiation (X-rays, γ-rays), energetic particles (electrons, protons, α-particles), UV light, high temperatures, combustion processes, reactive chemical reagents, mechanical stress, and explosions. As we shall see, under both these and other sets of conditions, structural dislocations may be introduced in the form of organic and inorganic free radicals, which host unpaired electrons, and their EPR signal may provide a marker of the kind of process that has created them. The great strength of EPR lies in its ability to identify the chemical nature of free radical species, and from the intensity and linewidths of the signal, it is possible to deduce the number of radicals that have been formed, along with various features of the local molecular environment in the sample.

Free radicals, moreover, play a central role in nature, particularly in living systems, and consequently, current activity in researching into these species is enormous. Mainly, this is because it is widely held, and this in part through the agency of EPR measurements, that radicals provide both the cause and mediation of many diseases, and indeed of the ageing process itself. The generally reactive character of radicals and unpaired-electron species generally (including metal ions, which can participate in redox processes) further underpins much of chemistry (it is, of course, 'chemistry' which is implicit to all the above), and it is largely on the findings from simpler chemical systems that much of current biochemical thinking is based, and this underlying free radical chemistry impacts further on a variety of environmental aspects – especially in the role of pollutants in atmospheric phenomena, such as ozone-loss, global warming and acid-rain production. Furthermore, since the atmosphere is in direct contact and exchange with the surface of the Earth – with the soil, the plants which grow within and upon it (biosphere), the rocks and mountains (lithosphere), and the rivers, seas and oceans (hydrosphere) – the chemistry of the

atmosphere takes on a wider role. Remarkably, EPR can provide insight into many of these phenomena too, both through its use in the investigation of model systems, and more directly as an analytical technique[15,46].

6.1.1 The basis of the experiment itself

The essential EPR experiment rests upon entirely similar principles to those which underpin NMR spectroscopy (Section 2), but the method is specific for detecting molecules with unpaired electrons – namely free radicals and certain metal (usually transition metal) complexes. EPR spectra are characterised by (*i*) g-factors (g-values) and (*ii*) hyperfine coupling constants, which are in analogy with (*i*) chemical shifts and (*ii*) spin–spin couplings in NMR.

A single unpaired electron has a spin, $s = \frac{1}{2}$, with quantum numbers $m_s = +\frac{1}{2}$ or $-\frac{1}{2}$. In the absence of an external magnetic field, both states have the same energy, and therefore, statistically, when a large number of unpaired electron species (free radicals or metal ions, *e.g.* Mn^{2+}, Fe^{3+}, Cu^{2+}) are present together in a given sample, there is an equal number of each state present (*i.e.* 50:50; $-\frac{1}{2}:+\frac{1}{2}$). When an external magnetic field is applied (Figure 11) this is no longer the case, and the energy of the $m_s = -\frac{1}{2}$ state is decreased, while that of the $m_s = +\frac{1}{2}$ state is increased, as a result of their interaction with the applied magnetic field. (As in the NMR case of the proton [Section 2.1], one can imagine the spinning electron behaving as a tiny magnet, which feels therefore, the influence of the far stronger external field.) The effect of the magnetic field B_0 on the two electron spin states may be represented by Eqn (4), where E_0 is the energy of both $m_s = +\frac{1}{2}$ or $-\frac{1}{2}$ states before the magnetic field is applied, and μ_B is the Bohr magneton (9.27408×10^{-24} JT^{-1}).

$$Em_s = E_0 + g\mu_B B_0 m_s \tag{4}$$

Thus an energy difference (ΔE) is introduced between the states $m_s = +\frac{1}{2}$ and $-\frac{1}{2}$, which is given by Eqn (5), and is seen to increase in direct proportion to the strength of the external magnetic field (B_0). In EPR, it is the g-factor (g-value) [given in Eqns (4) and (5)] that is quoted directly, as a variable parameter which renders a different ΔE for each type of radical, rather than quoting a chemical shift (δ) as is done in NMR. As with a nucleus in NMR, of course, the unpaired electron will resonate at a different magnetic field strength according to the kind of molecular species (radical or metal ion) that it occupies.

$$\Delta E = g\mu_B B_0 \tag{5}$$

This situation for EPR may be represented as in Figure 11, in which the external magnetic field has caused an energy level splitting between the levels associated with the $m_s = +\frac{1}{2}$ or $-\frac{1}{2}$ states. While helpful comparisons may be drawn between EPR and NMR, there are some essential differences, too. For example, as already described (and as is represented in Figures 2 and 11), in EPR it is the $-\frac{1}{2}$ level whose energy falls, while that of the $+\frac{1}{2}$ state increases: this reversal in behaviour with respect to the ^1H NMR experiment is due to the *negative* electron magnetic moment (Bohr magneton), μ_B, which partly determines the extent of the splitting, according

to Eqn (5), and so the energy levels are simply *reversed*. μ_B is also very much larger than μ_N, and so the energy level splitting is accordingly increased, and to the extent that microwave radiation is required to 'match' the energy level separation, rather than the radiofrequencies which are used in NMR. (For an external field [B_0] of 0.3 T, radiation of frequency *ca* 9.4 GHz [X-band] is required to match the EPR energy level separation, but only *ca* 13 MHz would be needed for ^{1}H NMR.) Due to the energy difference (ΔE) between them, the collection of unpaired electron spins is distributed between the two states $m_s = +\frac{1}{2}$ or $-\frac{1}{2}$, in relative populations that depend upon the Boltzmann distribution Eqn (6),

$$n(+\tfrac{1}{2})/n(-\tfrac{1}{2}) = \exp(-\Delta E/RT). \tag{6}$$

If the sample is exposed to a source of microwave radiation, whose energy *matches* ΔE, a resonance occurs with the unpaired electrons, in which those with spin $m_s = -\frac{1}{2}$ can absorb energy and are promoted (excited) to the higher energy $m_s = +\frac{1}{2}$ state (Figure 11), while their spin $m_s = +\frac{1}{2}$ counterparts can emit an equal amount of energy, and fall back to the $m_s = -\frac{1}{2}$ level. Since the microwave field is equally capable of stimulating a spin transition in either direction, if the populations of the two states were equal, there would be no overall effect of the 'resonance', since the absorption and emission of energy would simply cancel one another. But, because there is an overall excess of the $m_s = -\frac{1}{2}$ population, as noted earlier, there is a net absorption of energy. (This holds, so long as the relaxation mechanisms [which allow the return of the unpaired electrons in the excited state $m_s = +\frac{1}{2}$ to the ground state $m_s = -\frac{1}{2}$] are relatively efficient, so the process is *fast*. If the mechanisms are rather inefficient, or the microwave power level is very high, the two states rapidly become equally populated, and the signal intensity falls to zero. This condition is called 'saturation'.)
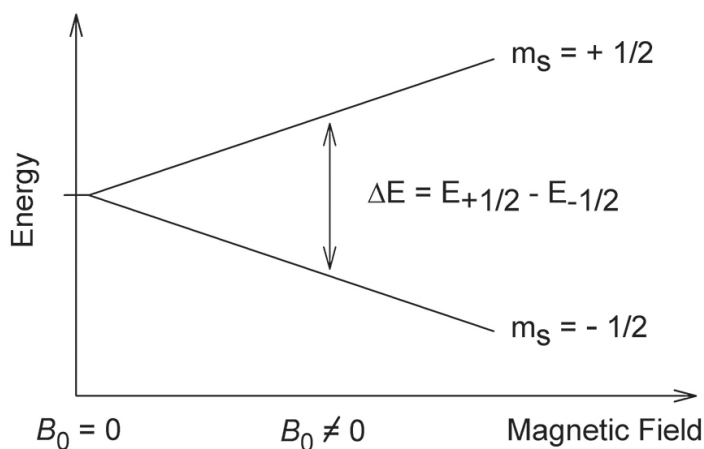

Figure 11 Splitting of electron spin energy levels by an external magnetic field (B) in an ESR experiment. Credit: By Astrochemist at English Wikipedia. http://upload.wikimedia.org/ wikipedia/commons/a/a9/EPR_splitting.jpg.

6.2 Molecular structural information that may be obtained from EPR

6.2.1 g-values

As noted in Section 6.1.1, in contrast to NMR, where a variable chemical shift (δ) is introduced, to account for the fact that protons in different electronic environments in molecules have slightly varying ΔE values (and hence, resonance positions), the convention in EPR is to quote the g-value directly, which varies depending on the type of radical (or metal ion), and so reflects the electronic environment of the unpaired electron. [Thus Eqn (5) is used for the 'resonance condition', rather than writing an expression analogous to Eqn (2), i.e. $\Delta E = g_e \mu_B B_0 (1 - \sigma)$, where g_e is the g-value for an isolated unpaired electron ('free spin') = 2.0023.] Either way, for both proton and electron resonances, the precise value of ΔE depends on the local electronic structure, and the resonance will occur at a different magnetic field strength (B_0), when a constant RF or microwave frequency (energy) is applied, since the energy level separation (ΔE) has to be 'tuned' by B_0 so that resonance can occur [Eqns (2) and (5)].

g-values for some representative species are listed in Table 2. The shift in g from the value for an *isolated* ('free') electron (2.0023, *no units*) is due to 'spin-orbit-coupling'. For organic radicals, g remains very close to the free-electron value, although it can be seen to increase when the spin becomes partially located on atoms with an increased nuclear charge (like O and N), and the shifts in g from free-spin can become quite pronounced for transition metal ions. This is due to the effect of spin-orbit coupling, as is discussed in the next section.

6.2.2 g-value variations

As noted above, g-values in radicals are generally shifted from that for a free electron ($g = 2.0023$). Moreover, these tend to vary as each of the *three x, y* or *z* (Cartesian) axes of the radical molecule is brought into alignment with the direction of the applied magnetic field; thus, in principle, *three* g-values, g_x, g_y, g_z, might be

Table 2 g-*values for selected free radicals and metal cations*

Species	g-value
Free electron (g_e)	2.0023
$CH_3\bullet$	2.0027[a]
$HOCH_2\bullet$	2.0034[a]
$MeC(=O)CH_2 \bullet$	2.0042[a]
$R_2N\text{–}O\bullet$	2.0058[a]
$RO\text{–}O\bullet$	2.015[a]
Cr^{3+}	1.98
Cu^{2+}	2.1–2.4
Ni^{2+}	2.25

[a]g-value measured for the radical in the liquid phase.

measured for a given radical (Table 3). [In liquid solutions, the radicals normally perform rapid reorientations, so that a single g-value (Section 6.2.1) is observed, which is the average of the three values that may be measured in a solid sample, where the molecules are restricted in their reorientation.] As noted, it is generally accepted that these variations arise from the phenomenon of 'spin-orbit coupling', although somewhat alternative descriptions have been used to account for the precise mechanism involved. The essential features responsible for a g-value shift (Δg) may be summarised[47] in Eqn (7),

$$\Delta g \propto \Sigma \rho_i \lambda_i / \Delta E_{i,} \tag{7}$$

in which Δg is the shift of any one of the principal g-components (g_x, g_y, g_z) from the free electron ('free-spin') value (2.0023). The overall shift is the sum of the contributions from all the atoms (i) in the radical. It is clear from Eqn (7) that the shift from free-spin will be larger if the unpaired electron population (spin-density) (ρ_i) increases on atoms (i) with large spin-orbit coupling constants (λ_i). Since the values of (λ_i) increase with increasing atomic number of atoms (i), Δg is expected to increase accordingly. This is sometimes called the 'heavy-atom effect', because the spin-orbit coupling constant (λ) increases roughly as the fourth-power of the nuclear charge ($\lambda \propto Z^4$), and so is most pronounced for radicals with 'heavy atoms'.

Spin orbit coupling is a magnetic coupling between the magnetism of the electron, arising from its spin, and magnetism acquired through its motion within molecular orbitals. It may be thought that the 'spin' keeps some of the 'orbital angular momentum' going, in a kind of magnetic induction effect. The induction of orbital angular momentum in a radical requires electronic excitation, involving the orbital containing the unpaired electron. This may take the form either of promotion of the unpaired electron to a vacant orbital, or of an electron from a filled orbital of lower energy into the unpaired electron orbital. The term ΔE_i in Eqn (7) represents the energy required for the excitation, in either situation, and may be thought to provide an 'energy barrier', which determines the amount of orbital angular momentum that may be induced by the unpaired electron 'spin'. The orbitals are thus 'magnetically coupled'. Since the orbital energies are different for each axis in respect to that of the unpaired electron orbital (ΔE_i), the induced angular momentum is also different for each axis and hence the g-components (g_x, g_y, g_z) have different values (Table 3).

Table 3 *Principal g-values for selected radicals*

Radical	g-values		
MeS–SMe$^+$•	2.036,	2.017,	2.002
MeS(H)-SMe •	2.059,	2.026,	2.002
RS–RS$^-$•	2.020,	2.011,	2.000
R$_2$S–SR$_2$$^+$•	2.022,	2.011,	2.004
EtSS•	2.042,	2.024,	2.002
RO–O •	2.035,	2.008,	2.003

Δg can be positive or negative, depending on the nature of the excitation, with that involving a filled orbital being positive and that with a vacant orbital being negative. The induced magnetic field can be thought to act in opposite senses, depending on the direction of induced electron spin-orbital motion.

In practice, one of the g-components usually remains close to the free-spin value (Table 3), while the shifts of the other two are determined mainly by the relevant energies and occupancies of the coupled orbitals. (In other words, the closer together a particular orbital is in energy with the unpaired electron orbital, and the greater the orbital coefficients of both, the more efficient is the coupling process and the larger is the g-shift.)

The isotropic g-value, observed from a rapidly reorientating radical, as in a liquid (Table 2), differs from free-spin (2.0023) by the average of the shifts corresponding to each Cartesian axis (x, y, z) of the molecule, Eqn (8).

$$g(\text{isotropic}) = [(\Delta g_x + \Delta g_y + \Delta g_z)/3] + 2.0023 \tag{8}$$

6.2.3 Hyperfine coupling constants

Where it may be observed, hyperfine coupling, the analogue of nuclear spin–spin coupling in NMR spectroscopy, is diagnostically the most useful feature of EPR, since it reveals the nature of magnetic nuclei that are present in a particular paramagnetic molecule. In order to appreciate this effect, we consider the simple
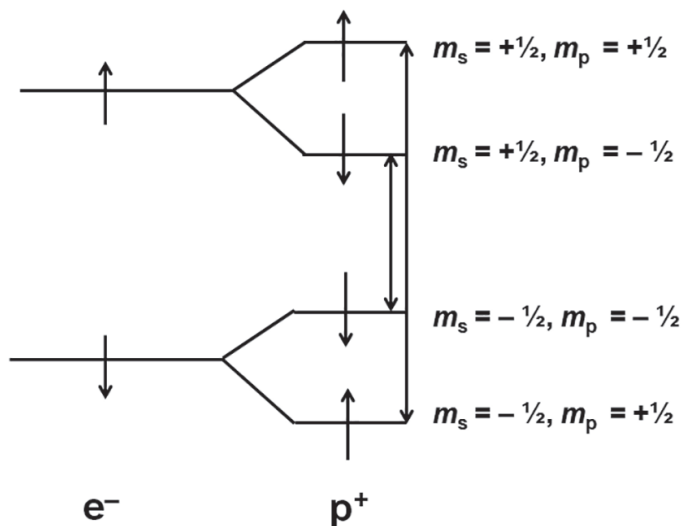

Figure 12 *Magnetic energy levels for a radical containing a single proton (R_2C–H): with hyperfine-coupled electron (e^-) spin states $m_s = +\frac{1}{2} -\frac{1}{2}$ and proton (p^+) spin states $m_p = +\frac{1}{2} -\frac{1}{2}$. As a result of the selection rule, that a nuclear spin cannot undergo reorientation ($\Delta m_I = 0$) simultaneously with the electron spin transition ($\Delta m_S = 1$), only the two transitions shown can occur, and so two lines are observed in the EPR spectrum. Reproduced by permission of John Wiley and Sons from ref. 93.*

example of a radical ($R_2C–H•$) with just one proton interacting with the unpaired electron. We need consider the $m_S = –½$ state of the electron since the EPR experiment measures the net absorption of energy due to the promotion of electrons from this to the $+½$ level. Accordingly, the associated proton may take either the $m_I = +½$ or $–½$ state with respect to this, and, as is depicted in Figure 12, the magnetism due to the intrinsic proton spin may either augment ($+½$) or detract from ($–½$) the applied magnetic field (B_0). Since, in first order, the quantum mechanical selection rules forbid the reorientation of a nuclear spin ($\Delta m_I = 0$) simultaneously with that of the electron spin ($\Delta m_S = 1$), only the two transitions shown can occur, and so two lines (doublet) are observed in the EPR spectrum.

Most radicals are more complex than this, and contain more interacting magnetic nuclei, for example the hypothetical radical, $R_2CHCHR•$, where the groups (R) contain no magnetic nuclei, and there are two inequivalently coupled protons (*i.e.* with different coupling constants). The situation is a simple development of that already discussed, and there is now a sequential splitting by the two protons of the initial electron spin energy levels. If the two protons have unequal couplings, the EPR spectrum will consist of four lines of equal intensity; however, if the sequential splittings are the same, two of the transitions are coincident: thus three lines are observed with relative intensities 1:2:1. The general rule is that if a group of (n) equivalent nuclei with spin (I) are coupled to the unpaired electron, $2nI + 1$ transitions and thus spectral lines will be observed. For the case of protons, or other nuclei with spin $I = ½$, this reduces to $n + 1$ lines for n equivalent nuclei, and the situation is therefore analogous to the familiar '$n + 1$' rule in NMR spectroscopy (Section 2.3.2). Thus the simplest organic radical $CH_3•$ gives four lines. The hyperfine couplings in EPR spectra are typically measured in units of magnetic field strength: in the older literature, the gauss (G) was used, but the mT (millitesla) is the unit most commonly used today (10 G = 1 mT). This contrasts with the convention in NMR, where the equivalent 'spin–spin' couplings are always quoted in frequency units (Hz).

6.2.3.1 Line intensities

As is the case in NMR spectroscopy, the relative intensities of the lines in a multiplet arising from the coupling of the odd electron with a set of n equivalent nuclei are given by the coefficients of the binomial expansion, and may conveniently be represented by 'Pascal's triangle' (Figure 5). Hence the four lines in the EPR spectrum of $CH_3•$ are in the ratio 1:3:3:1.

6.2.3.2 Coupling to different sets of n-equivalent nuclei

In this situation, as in NMR, the total number of lines to be expected from coupling of the unpaired electron with different sets of nuclei nx is given by $\Pi(2n_xI + 1)$ or, for nuclei with spin $I = ½$, by $\Pi(n_x + 1)$. To illustrate this, we may consider the case of the ethyl radical, $CH_3CH_2•$. This has two sets of protons $n_1 = 3$ and $n_2 = 2$: thus the formula predicts $(3 + 1)(2 + 1) = 12$ lines; the coupling constants are +27 G for the methyl protons and –22 G for the methylene protons. The form of the EPR spectrum can be developed in terms of a stick diagram (Figure 13); the line intensities shown
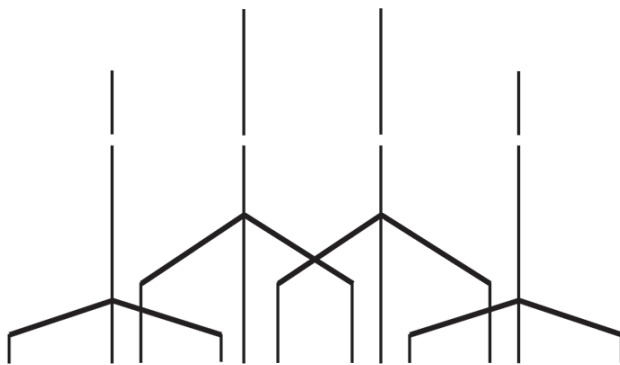
Figure 13 *Stick diagram showing EPR splitting pattern for the CH3CH2• radical. Reproduced by permission of Taylor and Francis Group, LLC, a division of Informa plc from ref 94.*

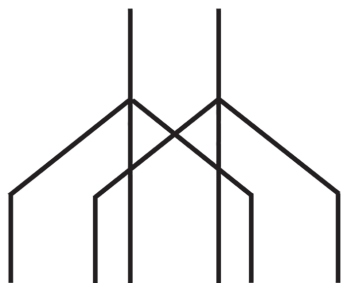**Figure 14** *Stick diagram showing EPR splitting pattern for radical PhRCHN(O•)Bu^t, showing coupling to a single proton (^1H) and one ^{14}N nucleus: a(^1H) < a(^{14}N). Reproduced by permission of Taylor and Francis Group, LLC, a division of Informa plc from ref. 94.*

are arrived at by splitting each of the 1:3:3:1 intense lines into three more of relative intensities 1:2:1.

6.2.3.3 Couplings to nuclei with I > 1/2

The most commonly encountered nucleus of this type is ^{14}N, with $I = 1$, so that it may take the values $m_I = +1, 0, -1$, with each state exerting its own magnetic influence on the unpaired electron, leading to a splitting of each electron m_S level into three. Three lines are therefore observed in the EPR spectrum, with a common spacing that is equal to the ^{14}N coupling constant. A radical often contains protons, in addition to the nitrogen atom, so that its EPR spectrum arises from the combination of the coupling with both kinds of nucleus. The number of lines, as always, can be derived from the formula $\Pi(2n_{XI} + 1)$, but the important case of a radical with the overall structure Ph(R)CHN(O•)Bu^t (as observed during spin-trapping experiments with PBN[48]) may be understood in terms of the coupling diagram (Figure 14), where it is assumed that the proton coupling is smaller than that of the ^{14}N nucleus.

6.2.3.4 Anisotropic hyperfine coupling

The foregoing refers explicitly to the simplified situation of radicals that are free to tumble rapidly in liquids (or in very mobile solid matrices such as adamantane). In many instances, particularly for reactive σ-radicals such as phenyl, or almost all radical ions other than highly delocalised species usually derived from aromatic molecules, it is necessary to use matrix isolation methods. In the normal event, the tumbling rates of radicals isolated in solid matrices are relatively low, and the effects of the anisotropic magnetic dipolar nucleus–electron couplings are manifested in the EPR spectrum (see Section 6.2.3.5). (Typically, the g-factor is also anisotropic, but for radicals centred on first-row elements this normally provides a relatively minor influence on the spectra.) In situations where the tumbling rate is intermediate between that typical for radicals in liquids or in solids, line-broadening occurs from which motional information may be extracted (see Section 6.4.1).

6.2.3.5 Anisotropic coupling to the nucleus of the radical centre

This is best illustrated with an example; that of the hypothetical amine radical cation $R_3N^{+}\bullet$. This is isoelectronic with the corresponding alkyl radical $R_3C\bullet$, but has the advantage that the magnetic central atom (^{14}N) nucleus is in nearly 100% of natural abundance and so its influence dominates the EPR spectrum (it is assumed that the groups R contain no strongly coupled magnetic nuclei and thus give no hyperfine splittings). In essence, there are two extremes: (*i*) in which the radical is oriented so that the projection of the $N(2p_z)$ orbital is parallel ($\parallel$) to the applied magnetic field (B_0) (along z); and (*ii*) in which the orientation is perpendicular ($\perp$) to (B_0); it may be recognised that there are two equivalent axes (x,y) for which the latter is true. In the former case, the parallel coupling ($A_\parallel$) is the maximum possible, since the anisotropic (dipolar) coupling ($2B$) from the ^{14}N nucleus takes the same (positive) sign as the isotropic coupling (a), as shown by Eqn (9).

$$A_\perp = a + 2B \tag{9}$$

In the latter case, the dipolar coupling is only half the value (B), and of opposite sign, so that there is a net cancellation of effects, Eqn (10), which for nitrogen centred π-radicals leads to values for the perpendicular coupling (A) close to zero.

$$A_\perp = a - B \tag{10}$$

If the radicals are formed in a single crystal environment so that they are mainly all aligned with respect to the crystal axes, then rotation of the crystal about these x, y, z axes leads to a simultaneous shift in the positions of the outermost two lines of the $I = 1$ triplet which will pass through the maximum and minimum positions (Figure 15a and b, respectively). On the other hand, in a randomly matrix isolated system, as is more commonly encountered, there is no such overall alignment and so the resulting EPR spectrum is a composite of the spectra taken over all orientations, and the entire range of couplings intermediate between $A_\parallel$ and $A_\perp$ is encompassed, leading to the characteristic solid-state 'envelope' shape (Figure 15c). When

the first derivative of this pattern is measured (Figure 15d), as is normal for EPR spectrometers, the parallel and perpendicular features stand-out as shown, although for ^{14}N π-radicals the perpendicular peaks are often coincident with the parallel $|0>$ line (Figure 15e) because the perpendicular coupling $(A_\perp)$ is close to zero, and in the absence of splitting merely lends intensity to this central line, leading to a very prominent central feature; however, the direct admixture of s-character in a ^{14}N σ-radical usually renders the perpendicular features visible (due to the increase in $A_\perp$ by the larger isotropic component $[a]$), since we may deduce [from Eqn (11)], that $A_\perp = (3a - A_\parallel)/2$.

The fact that $A_\parallel$ and $A_\perp$ often can be determined by direct inspection of the powder EPR spectrum is extremely important because, from these, estimates of the s and p orbital populations at the radical centre may be obtained by means of Eqns (11–14), (the discussion given here for nitrogen centred radicals holds true for most other elements, although corrections for orbital magnetic contributions are necessary for heavier elements and for transition metal complexes).

$$a = (A_\parallel + 2A_\perp)/3 \tag{11}$$

$$\%s = (a/a_0) \times 100 \tag{12}$$

The isotropic coupling (a), while not measurable directly from the solid state spectrum, can be estimated from Eqn (11), and the pure dipolar coupling $(2B)$ from Eqn (13).

$$2B = A_\parallel - a \tag{13}$$

$$\%p = (2B/2B_0) \times 100 \tag{14}$$

Since values have been tabulated in the literature, as calculated from appropriate atomic wave functions, for the coupling constants expected for unit occupancy of a particular s (a) or p $(2B_0)$ orbital, these may be used in Eqns (12 and 14) to map out the unpaired electron distribution over these orbitals.

6.3 EPR Instrumentation

6.3.1 Multi-frequency EPR[49]

The microwave radiation used in EPR is most commonly of frequency *ca* 9–10 GHz [*i.e.* $(9 - 10) \times 10^9$ s^{-1}] – termed 'X-band' – but other frequency ranges are sometimes employed. When a different choice of microwave frequency is made, a different strength of the external magnetic field is required to achieve the resonance condition. This follows from Eqn (5), according to which it is also clear that as the frequency decreases, a smaller excess spin-population occurs in the ground state $n(-\frac{1}{2})$. Since the innate sensitivity of EPR depends on the ratio $n(+\frac{1}{2})/n(-\frac{1}{2})$, which relates to the Boltzmann factor [Eqn (6)], it is clear that measurements made at lower microwave frequencies will afford an intrinsically weaker signal. There
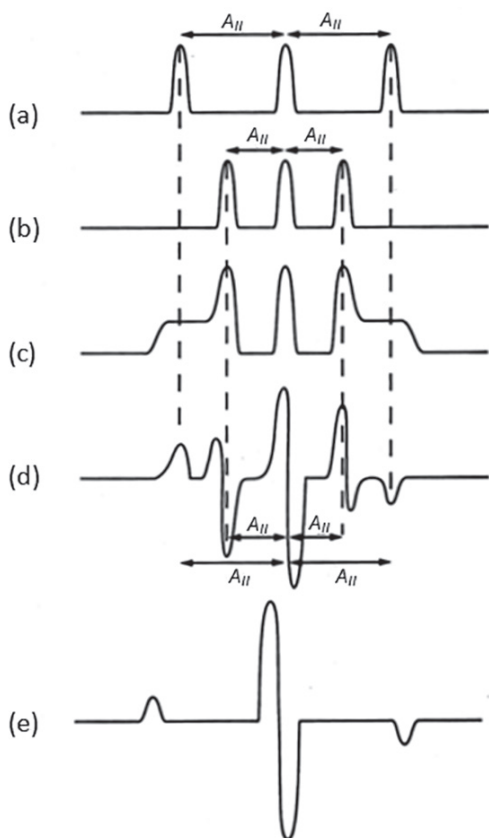
Figure 15 Illustration of anisotropic coupling to the ^{14}N nucleus in a radical $R_3N^+\bullet$. Reproduced by permission of Taylor and Francis Group, LLC, a division of Informa plc from ref. 94.

are, however, very good reasons for undertaking so called 'multi-frequency' experiments. For example, in the study of large biological or aqueous samples (including isolated organs, such as the liver, and whole, small animals), a frequency of *ca* 1.5 GHz ('L-band'), or even lower than this, is often beneficial. This is because the absorption of microwave radiation by water becomes increasingly attenuated on reduction of its frequency from the 'X-band' region. It is also important to be aware of the 'dimensions' attendant to the experiment: namely the size of the resonant cavity. At X-band, the frequency (v) is *ca* 9.5×10^9 s^{-1}, which corresponds to a wavelength (λ) of 3.2 cm. In order to set-up a resonant (standing) wave, the cavity must also be of this dimension. At L-band, since $v = 1.5 \times 10^9$ s^{-1}, the size of the cavity is now 20 cm (8 inches), and so a far larger sample might be accommodated. Allowing, overall, for the loss of sensitivity caused by the reduced Boltzmann factor at the lower frequency, and the compensation for this that is possible with a much larger sample volume, a working rule is that an L-band experiment is of around a factor of 10 lower in sensitivity than one at X-band. Similar reasoning applies to measurements made at higher frequencies. For example, at W-band, $v = 9.4 \times 10^{10}$ s^{-1}. In this case, $\lambda = 0.32$ cm (*ca* 3 mm), and the sample is usually contained in a tube of overall diameter *ca* 1 mm, with an internal diameter of *ca* 0.6 mm. While it is

Table 4 *Frequency ranges, wavelengths and resonant magnetic fields for different microwave bands*

Band	v (GHz)	λ (cm)	B (G)
L	1.5	20	500
S	3	10	1,000
X	9.5	3.2	3,400
K	24	1.3	8,500
Q	35	0.8	12,100
W	94	0.3	33,500
D	140	0.2	49,000

true that the experiment is ideal for (highly expensive) biological materials, available only in small quantities, and that the greatly increased Boltzmann factor will to some extent offset the loss of sensitivity from such a small sample, the actual signal intensity is limited by problems of magnetic field inhomogeneity and component construction. The commonly encountered microwave frequencies, their wavelength equivalents and attendant magnetic fields required for resonance, are all listed in Table 4, although we note that EPR experiments have been done at frequencies up to *ca* 500 GHz.

Multi-frequency methods are generally resorted to in an effort to improve the resolution of a given EPR spectrum. In the solid state, it is sometimes unclear whether an apparent splitting arises from different g-components, or is due to hyperfine coupling. By increasing the frequency, the separation of g-components is increased, but a hyperfine splitting will be unaffected. In other cases, g-components may not be fully resolved, but become so at a higher frequency. (The effect is in precise analogy with the increased separation of chemical shifts that is obtained at higher frequencies/fields in NMR spectroscopy; Section 2.1.)

A range of frequencies from Table 4 has been applied to a frozen sample containing a nitroxide, in which the radical molecules tumble only slowly, the results of which are evident in Figure 16. At X-band (9 GHz), the triplet splitting from ^{14}N in the 'parallel' direction is clear, but there is no resolved 'perpendicular' ^{14}N splitting on the central feature. Nor are any of the g-components resolved, because the g-anisotropy provides only a very small splitting at this relatively low frequency. However, as the frequency is increased, there is a progressive separation of the g-components, until, at D-band (140 GHz), they are fully resolved. The parallel splitting is now clear on the highest-field g-feature, and incipient (perpendicular) splitting is now evident on both the other g-features if they are inspected closely. At the lower frequencies, overlap between these components diffuses their detail into the linewidths. In other experiments, this time for rapidly-tumbling nitroxides, used to probe a distribution of aqueous and lipid phases present simultaneously in a given sample, the two environments are readily identified at W-band, since a smaller isotropic g-factor is conferred to a nitroxide in the aqueous medium, while
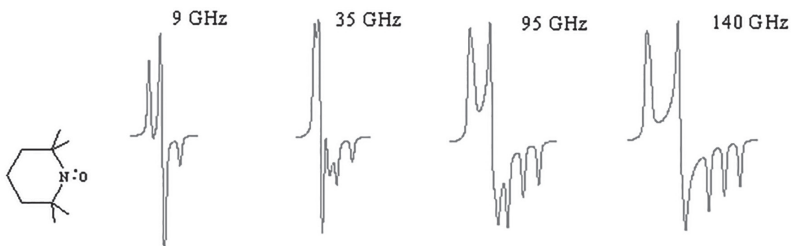
Figure 16 ESR spectra of a nitroxide in a solid frozen medium, recorded as a function of the frequencies shown. Credit: Astrochemist. http://upload.wikimedia.org/wikipedia/en/8/8e/ EPR_multifrequency_spectra.jpg.

the isotropic ^{14}N coupling is simultaneously increased. Thus two separate spectra are visible from the two environments. At X-band, there is often considerable overlap between the signals from the two components[15].

6.3.2 In-vivo *EPR*[50]

By means of low-frequency EPR, *e.g.* at L-band or lower, it is possible to examine biological samples including whole animals, or, say, the arm of a human volunteer (or the leg, if they are sufficiently thin). For the most part, stable nitroxides have been introduced into animal subjects (rats and mice) which can be detected *in vivo*. Human subjects have mostly been studied from the point of view of oximetry[15], *i.e.* to measure the oxygen concentration in tissue using the paramagnetic line-broadening that is caused by Heisenberg spin-exchange between the unpaired electrons in stable free-radicals present in the tissue, *e.g.* skin, and those in dioxygen molecules, which have a triplet electronic state (two unpaired electrons). One experimental arrangement is still under development, for performing oximetry on whole human subjects which has a 50 cm cavity[50].

In vivo EPR has also been used to determine high radiation-dose exposures, from the signals engendered in tooth enamel[50]. As a result of terrorism, accident or war, there is the potential risk that populations might be exposed to doses of ionising radiation sufficient to cause direct clinical effects within days or weeks. Thus, there is a critical need to determine the magnitude of the exposure to individuals so that those with significant risk can have appropriate procedures initiated immediately, while those without a significant probability of acute effects can be reassured and removed from the need for further consideration by the medical/emergency team (*i.e.* to establish a triage system). It is extremely unlikely that adequate dosimeters will be worn by the potential victims, and nor is it probable that prompt and accurate dose reconstruction will be possible on an individual basis. *In vivo* EPR measurements of radiation-induced changes in the enamel of teeth provide perhaps the only method able to differentiate among doses sufficiently to classify individuals into categories for treatment with enough accuracy to facilitate decisions on medical treatment. In its current state, the *in vivo* EPR dosimeter can provide estimates of absorbed dose in the 1–10 Gy range. Both the lower limit and the precision are expected to

improve, with better resonators and algorithms for acquiring and calculating the dose. However, even in its current state of development, the method is nonetheless good enough to decide among individuals with regard to acute effects from exposure to ionising radiation for most applications related to terrorism, accidents or nuclear warfare.

6.3.3 Pulsed EPR

Pulsed EPR[51] is a magnetic resonance technique in which a microwave pulse provides a short oscillating field which is used to perturb the alignment of the net magnetisation vector of a collection of electron spins in a static magnetic field. A microwave signal is emitted, which by Fourier transformation gives rise to a frequency domain EPR spectrum. Thus, the method is in analogy with FT NMR (Section 2.2.2). With a vast variety of pulse sequences it is possible to gain extensive knowledge regarding structural and dynamical properties of paramagnetic compounds. While conventional (CW) EPR and ENDOR methods can provide a variety of information regarding the unaired electron distribution for different kinds of paramagnetic species, the spectral and time resolution that they can provide is limited. However, using pulsed EPR it is possible to investigate various magnetic interactions at greater resolution, by making an appropriate choice of pulse sequences. The year 1958 was pivotal for pulse EPR, since this is when an electron spin echo was first observed (from a sample of sodium dissolved in ammonia at ambient temperature)[51], and also the first microwave electron spin echoes from dopants in silicon were detected using a excitation frequency of 23 GHz. The first observation of electron spin echo envelope modulation (ESEEM) was made in 1961 by Mims, Nassau and McGee, working at Bell Labs, and the Mims group also first reported the phenomenon of pulsed electron nuclear double resonance (ENDOR) in 1965[51]. The first commercial pulsed EPR and ENDOR spectrometers, which operated at X-band frequencies, appeared in the 1980s, and in the following decade, the first commercially available W-band ENDOR spectrometer appeared[51].

Far shorter pulse lengths are required in EPR than in NMR (due to the very short electron spin relaxation times, as compared with those from nuclei). It is also the case that the entire EPR spectrum cannot usually be excited by the available bandwidth. However, while noting these limitations, a variety of proven and powerful spectroscopic methods[52] has been developed based on pulsed EPR, which use time-domain and multi-dimensional techniques, and can provide information that could not be obtained using CW methods. Pulsed EPR and its ancillary techniques are of particular value in determining structural details of complex biological molecules, *e.g.* proteins. The advantages of performing pulsed EPR at different microwave frequencies have been discussed[53].

6.3.3.1 Electron spin echo envelope modulation (ESEEM)

When a multi-pulse sequence is employed to produce a spin echo, its amplitude decays as a function of the delay between pulses, as a result of relaxation processes in the system. Quite frequently, modulation of the spin echo is observed, which

is a consequence of weak hyperfine interactions with nuclear spins (and that the $\Delta m_I = 0$ selection rule is no longer entirely valid). The method reveals the identity of particular coupled nuclei and allows a determination of small hyperfine, and quadrupole couplings, which are useful pieces of information in devising structural models of often complex systems.

6.3.3.2 Hyperfine sub-level correlation spectroscopy (HYSCORE)

This is a 2D experiment based on the ESEEM effect, which provides a determination of correlations between the magnetic frequencies of nuclei in the different electron spin manifolds (*e.g. m_s* = +½ and –½), and so assists in the interpretation of EPR spectra which contain a number of different overlapping signals.

6.3.3.3 Electron nuclear double resonance (ENDOR)

Pulses of both microwave and radiofrequency radiation are used in this form of spectroscopy: the electron spin echo is monitored as a function of a radiofrequency pulse which pumps the nuclear spin transition(s). The method permits the measurement of hyperfine interactions that are larger than can be measured using ESEEM but which are below the resolution of CW EPR.

6.3.3.4 Double electron–electron resonance (DEER)/pulsed electron double resonance (PELDOR)

Pulses of microwave radiation are employed at two different frequencies in DEER: the modulation of an electron spin echo generated by the first pulse is monitored as a function of a second microwave pulse, which due to its different frequency, causes a different set of spins to flip. The change in the second set of spins affects the field felt by the first set (which are giving rise to the spin echo). This allows the determination of very weak dipolar interactions between remote electron spins to be determined, which is extremely useful in various applications in biology and materials science, especially when employed in combination with spin labelling techniques.

6.4 Applications of EPR

As we have seen, in principle, NMR spectra may be recorded from dozens of different nuclei, whereas obtaining an EPR spectrum requires some of the sample molecules to contain one or more unpaired electrons, which might appear to be an oddity. Notwithstanding, here lies the beauty of EPR, since the method is completely specific for unpaired electrons, which are frequently formed in materials that have encountered one or more of a range of important energetic conditions (as noted in Section 6.1), for which a signature is supplied in the form of the consequent EPR spectrum. The unpaired electron bearing sites are usually termed 'damage centres', 'defects' or 'trapped electrons' by physicists, geologists, archeologists and environmental scientists, but are normally referred to by chemists and biologists as 'free radicals', whose detailed molecular structures may be revealed from the spectral parameters of hyperfine splitting (Section 6.2.3), where it is observed, and of *g*-value (Section 6.2.2).

Paramagnetic transition-metal cations, *e.g.* Fe^{3+}, Mn^{2+}, Cu^{2+}, are quite commonly detected in environmental samples and in biological tissues using EPR. Paramagnetic materials, including metal cations and synthesised complexes or stable organic radicals (usually nitroxides), may be deliberately added to samples as probes of local molecular environments such as cell-membranes, and to determine their dynamic properties. Along with other stable 'organic' radicals (*e.g.* carbon chars and lithium phthalocyanines), nitroxides may be used to measure oxygen tensions in whole tissues and in simpler cellular systems. Metabolic activities in such biological media may also be determined from the reduction kinetics of nitroxides. When it is desired to investigate various reacting systems for the intermediacy of free radicals, 'spin-traps' are often added[48]. These are frequently of a structural type designed to 'trap' reactive radicals by addition to them, so forming nitroxides *in situ*, which rise to detectable concentrations in consequence of their relative stability. Clearly, there are many and varied important applications for EPR, and most importantly so in areas of the biological[15] and environmental sciences[46].

6.4.1 Spin-labelling

6.4.1.1 Background to method

Essentially, this technique[54] involves the incorporation of a stable radical, usually a nitroxide, into a medium as a probe of molecular mobility, and rests upon the averaging of anisotropic *g*- and hyperfine tensors, as is illustrated in Figure 17. (In such experiments, the stable radical is often termed a 'spin probe'.) At one extreme is the limit of fast motion, where the molecules are tumbling very rapidly and the anisotropies of the tensors are completely averaged, and the spectrum shows three lines of equal intensity, spaced by the isotropic ^{14}N coupling constant and centred on the isotropic *g*-factor. The intermediate situation is called the region of 'intermediate motion' where the anisotropies are not completely averaged, but their presence results in an asymmetric broadening of the lines, as shown, being greatest for the high field line. By a detailed analysis of these lineshapes, it is possible to derive the rate of motion of the probe and thus the local degree of motion of its environment.

As described above, the onset of such rotational motion causes the three lines to appear with differing intensities and widths. The EPR spectrum is insensitive to molecular motion faster than *ca* 10^{-12} s, but that occurring on a timescale of *ca* 10^{-9} $< \tau_c < 10^{-11}$ s, results in line broadening. From the relative intensities (heights) of the lines associated with the +1, 0, –1 nuclear spin states, V_{+1}, V_0, V_{-1}, the width of the central line ΔH_0, and Eqns (15) and (16), values for the rotational correlation time τ_c of the radical can be estimated[15]. When the reorientational motion is isotropic, Eqns (15 and 16) should give the same answer, but their estimates will differ when there is anisotropy present, *i.e.* the probe tumbles more rapidly about one axis than the others.

$$\tau_c = 6.6 \times 10^{-10} \Delta H_0 [(V_0/V_{-1})^{1/2} + (V_0/V_{+1})^{1/2} - 2] \tag{15}$$

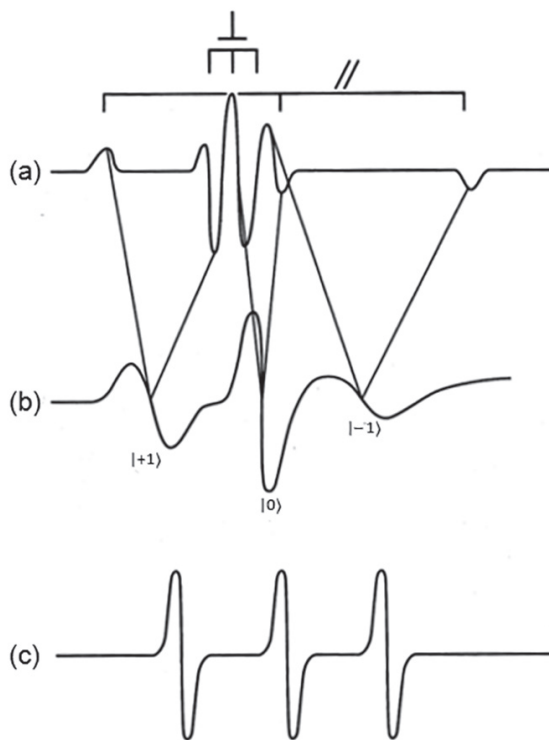$$\tau_c = 6.6 \times 10^{-10} \Delta H_0 [(V_0/V_{+1})^{1/2} - (V_0/V_{-1})^{1/2}] \tag{16}$$

Figure 17 *Idealised EPR spectrum of a spin-label (R₂N–O•): (a) in the limit of slow motion (with resolved* $g_\perp$ *and* $g_\parallel$ *and* ^{14}N $A_\parallel$ *and* $A_\perp$ *components fully resolved), (b) line broadening in the region of intermediate motion (due to partial averaging of the features shown), (c) the limit of fast motion (where the g- and A- components are fully averaged). Reproduced by permission of Taylor and Francis Group, LLC, a division of Informa plc from ref. 94.*

The nitroxide may simply be dissolved in an appropriate medium, to probe its viscosity, since the correlation time is directly related to the viscosity η according to Eqn (17); it is also clear that as molecules become larger (r is their radius), or if the viscosity of the medium (η) increases, they move more slowly (in accord with common sense).

$$\tau_c = 4\pi\eta r^3/3kT \qquad (17)$$

In studies of proteins, or of membranes, the nitroxide is chemically attached to a molecule whose motion it is desired to study; in this case, the motion of the nitroxide (spin label) reflects the motion of the fragment to which it is attached (Figure 18). Particularly in this kind of situation, the motion is anisotropic, and complex theoretical models must be applied to analyse the spectra, leading to details of the type of motion and its rate about each axis. At sufficiently high concentrations, nitroxides can be used to probe lateral (translational) diffusion, on the basis of the line broadening which results from the interactions between the unpaired electrons in two radicals which have diffused together.
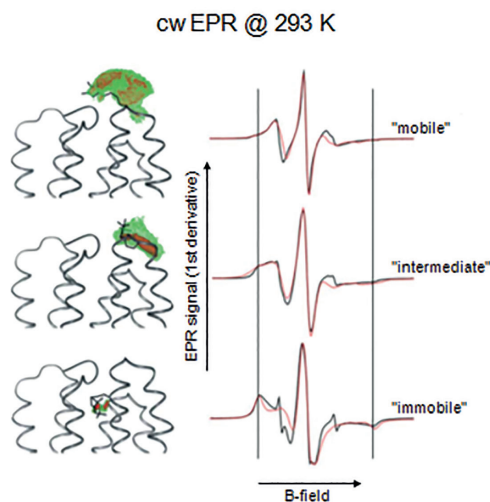
cw EPR @ 293 K

EPR signal (1st derivative)

"mobile"

"intermediate"

"immobile"

B-field

Figure 18 *Nitroxide (spin label) bound to a protein: influence of molecular motion on ESR spectrum. Continuous wave (CW) spectra measured at 293 K.* **Credit:** *Dr Enrica Bordignon.*

6.4.1.2 Spin-labelling studies of membranes

The literature on spin-labelling studies of membranes is enormous and covers many diverse aspects of membrane function and biochemistry; however, the following discussion intends to illustrate some of the important advances made in the understanding of membrane properties using spin-labelling techniques. As an introduction to this field, we call attention to an excellent review[55] of magnetic resonance studies of membranes, which includes both spin-labelling and NMR work. Membranes provide highly anisotropic environments, due to the regular arrangement of their constituent molecules, each with its own anisotropic properties. The molecular packing in lipid membranes varies from the tight orthorhombic lattice of the L_c phase, to the loose and hexagonal packing of molecules in the liquid crystalline L_α phase. Micro-viscosity differences of many orders of magnitude between these phases (which is almost like a solid crystal in L_c, but similar to a liquid in L_α) confer similarly large differences in the motional rates for lipid molecules. EPR methods are of particular aid in studying membrane molecular motion, since they are sensitive over the relevant millisecond to nanosecond timescales involved, which are also the timescales of numerous biological events. Almost certainly there is close connection between membrane function and molecular motion, of which there are three main kinds that may be determined by EPR for lipids, described as, angular rotation, lateral diffusion and trans-bilayer movement (also termed flip-flop). This is an extremely important field, which has been surveyed in some excellent reviews[56,57].

6.4.1.3 Selected examples

A model previously developed for describing the dynamics of flexible alkyl chains has been adapted to the analysis of spin-label spectra obtained from an oriented

phospholipid membrane: in this model, rotation around each C–C bond of the labelled alkyl chain is characterised by two inequivalent minima, with one end of the chain fixed to mimic the phospholipid headgroup, and with the dynamic effects of the nitroxide label included explicitly. This model is integrated with that for the overall rotation of the phospholipid in the mean orientational potential of the aligned membrane, and it is incorporated into the stochastic Liouville equation which describes the EPR lineshape in the presence of these dynamic processes. The analysis is simplified by introducing the fact that the relatively rapid internal modes of motion can be treated by motional narrowing theory and a time scale separation can be made with respect to the much slower overall motions of the phospholipid. A series of EPR spectra from the spin-label 16-PC in the lipid dimyristoylphosphatidylcholine were obtained in the range of temperature 35–65 °C in the L_α phase for various orientations of the normal to the bilayer plane relative to the magnetic field. Very good agreement with the experimental data is obtained from this model by using a least squares fit procedure[58].

Another paper by this group reports[59] a study of lipid-gramicidin interactions using 2D Fourier-transform EPR. It is shown that 2D-FT EPR spectra provide substantially enhanced spectral resolution in respect of changes in the dynamics and ordering of the bulk lipids – as compared with continuous-wave (CW) EPR – that result from addition of gramicidin to membrane vesicles of phosphatidylcholine in excess water containing 16-PC as the lipid spin-label. Both the rotational and translational diffusion rates of the bulk lipid are substantially decreased by addition of gramicidin (GA), whereas the ordering is only slightly increased, for a 1:5 ratio of GA to lipid.

No significant evidence is found in the 2D-FT EPR spectra for a second immobilised component, which is seen in CW EPR measurements, and simulations of the FT spectra suggest that this component, usually ascribed to 'immobilised' lipid is inconsistent with its being characterised by increased ordering, but is more consistent with a component with a significantly reduced diffusion rate. This is because the 2D-FT EPR spectra exhibit a selectivity, which favours components with longer homogeneous transverse relaxation times.

2D-FT and CW EPR spectra at X-band frequencies were recorded over a broad range of temperatures covering the solid and melt states of a liquid crystalline polymer. The CW spectra were analysed using conventional motional models. The nematic phase was macroscopically aligned in the magnetic field, whereas the solid state showed microscopic order but macroscopic disorder; an end label on the polymer showed smaller ordering and larger reorientational rates than those for the cholestane spin-probe dissolved in the same polymer, since the former can reorient by local internal chain modes. It was demonstrated that the 2D-FT EPR experiments provide greatly enhanced resolution to the order and dynamics of the end label, especially when performed as 2D-ELDOR (electron–electron double resonance) experiments as a function of the mixing time. Instead of the conventional model of Brownian reorientation, a model of a slowly relaxing local structure which enables

differentiation between the local internal modes experienced by the end label and the collective reorganisation of the polymer molecules around the end label, yielded much improved fits to the experiments in the nematic phase[60].

Lipid–protein interactions play a major role in the functioning of a biological membrane. It has been found that the stoichiometries of lipid–protein interactions, obtained from spin-label EPR experiments with integral membrane proteins, deviate from values predicted from simple geometric models for the intramembranous parameter that are based on the predicted numbers of transmembrane helices: these deviations provide evidence for oligomerisation of the protein in the membrane and/or the existence of more complex arrangements of the transmembrane segments[61].

The specific binding of hen egg white avidin to phosphatidylcholine lipid membranes containing spin-labelled N-biotinylphosphatidyethanolamines was investigated by EPR[62]. Spin-labelled derivatives were prepared with the nitroxide group at position C-5, C-8, C-10, C-12 or C-14 of the lipid chain, and binding of avidin caused a strong and selective restriction of lipid mobility at all positions of labelling. Overall, the results indicate that the biotinylphosphatidylethanolamines are partially withdrawn from the membrane, with a vertical displacement of 0.7–0.8 nm, on complexation with avidin.

Conventional EPR of spin-labelled lipids and saturation-transfer EPR of spin-labelled proteins are used to study lipid–protein interactions and the mobility of integral proteins, respectively, both in biological membranes and in reconstituted lipid–protein systems. Conventional EPR reveals two spin-labelled lipid populations, the mobility of one being hindered by direct interaction with the integral membrane proteins[63]. The proportion of the latter component increases with increasing protein content and with increasing selectivity of the lipid species for the protein. Lipid exchange rates at the protein interface obtained by spectral simulation are found to be consistent with fast-exchange, as found by ^{2}H NMR on similar systems, and to reflect the lipid selectivity observed by EPR. Protein-reactive covalent labels were used to study the rotational diffusion and aggregation states of membrane proteins *via* saturation-transfer EPR. The integral protein rotation is uniaxial and the anisotropic motion is analysed to obtain the principal component of the diffusion tensor: this is sensitive to the cross-sectional dimensions of the protein in the membrane, and hence to its state of assembly. A variety of novel experiments based on the power saturation properties of the spin-labelled components were also used to determine lipid exchange rate, protein translational diffusion rates, and the location and penetration of proteins in membranes.

Finally, we mention the use of W-band EPR in a determination of the partitioning and dynamics of 2,2,6,6-tetramethyl-1-piperidinoxyl nitroxide radicals in large unilamellar liposomes. The nitroxide was completely resolved in both lipid and aqueous phases on account of the large separation of its differing isotropic *g*-values in the two media[64].

7. Muon spin resonance (*µ*SR)

We are quite familiar with the isotopes of hydrogen known as protium ('ordinary' hydrogen), deuterium and tritium, each of which has one orbital electron and a single proton in its nucleus, the latter acting as an electrostatic counterweight to render the atom overall electrically neutral. These isotopes differ in the order listed above by the addition to the nucleus of zero, one and two neutrons, respectively. Both protium and deuterium are stable, whereas tritium undergoes radioactive decay with a mean lifetime of 17.7 years. Muonium is in a singular category as a hydrogen isotope, since its nucleus contains neither proton nor neutrons but consists solely of one positive muon. Like tritium, muonium is radioactive since the nuclear muon undergoes radioactive decay, but it is far more short-lived than tritium, and has a mean lifetime of just *2.2 microseconds*. By implantation of positive muons in the form of a beam from a particle accelerator into a variety of materials, muonium atoms and free radicals are created[9,65,66].

In addition to its property of radioactive decay, the muon also has spin, and therefore experiments akin to those of conventional magnetic resonance[7,8] may be undertaken. Hence in the various names given to the techniques that may be employed using muons, *µ* stands for muon and *S* for spin, while *R* may refer to rotation, relaxation or resonance. Although the title 'muon spin resonance' has been chosen above to provide a clear analogy with NMR and EPR, the principal techniques employed in *µ*SR are normally referred to in the literature as transverse field muon spin rotation (TF *µ*SR), avoided level crossing muon spin resonance (ALC *µ*SR) (sometimes also called muon level crossing resonance) and longitudinal field muon spin relaxation (LF *µ*SRx). However, the experiments which are rendered possible by muons are *unique*, and have no exact counterpart in more conventional magnetic resonance methodologies. In particular, that single-particle-counting methods are used in combination with samples in which nuclear spins are 100% polarised (*i.e.* vastly in excess of the Boltzmann factor!) permits unparalleled sensitivity regarding reactive radicals. Through the methods of *µ*SR, knowledge of radicals in various media has been gleaned that would have been denied to the more conventional approaches of EPR, and its related methods[7,15,46]. In order to do such experiments, it is necessary to obtain access to one of the several muon facilities which are distributed around the world, particularly the Paul Scherrer Institute (PSI; Switzerland); the ISIS pulsed-surface muon facility at the Rutherford Appleton Laboratory (RAL; UK); TRIUMF (Canada) and KEK (Japan). Most of the work that I have been involved with personally was done at PSI and RAL, with some collaborative ventures at KEK. As is usual with sophisticated techniques, chemists (and other kinds of scientists) have borrowed *µ*SR from the physicists, and it is the latter who remain by far the greatest in number as muon users. Nonetheless, muon *chemistry* has been active for around three decades, and much insightful data has been gathered through its agency. Originally, the kinetics and structural studies of radicals were of paramount focus, and while these remain important topics, unique investigations of free-radical processes occurring on reactive surfaces have been undertaken in an effort

to comprehend the involvement of radicals as reactive intermediates in catalysis by zeolites, and in reactions of pollutants on solid atmospheric aerosols. Related results for some environmentally significant[67] microporous media have been reported, including clays, porous carbons, porous silica and some preliminary work on porous ice-surfaces.

7.1 Muonium as a radiolabel

Muonium, a radioactive hydrogen atom with a positive muon as its nucleus, is formed *in situ* in materials when they are irradiated with positive muons (μ^+). Thus the method is one of radiolabelling, and is used extensively in mechanistic and kinetic studies of molecular processes[65,66]. As an isotopic *hydrogen* label, tritium (^3H) is often used, since its nucleus has spin ($I = \frac{1}{2}$), and so NMR experiments are feasible, and being also radioactive, it may be detected by scintillation counting of the β-particles (electrons) produced in its decay Eqn (18)[68].

$$_1^3H \rightarrow \ _2^3He + e^- + \overline{\nu}_e \qquad (18)$$

Indeed, ^3H is usually considered *the* radioisotope of hydrogen. Since the muon is radioactive also being a β-emitter [Eqn (19)], muonium atoms, either free or as bound in molecules, may similarly be detected by scintillation counting; it is, however, a positively charged electron (*positron*) which is produced, since μ^+ is 'anti-matter'! Therefore, the positive muon is also sometimes referred to as an 'antimuon'. The negative muon is sometimes simply called the 'muon'.
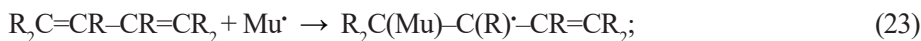
As noted, the positive muon (μ^+) – the radioactive nucleus of muonium – is relatively short-lived, having a *mean lifetime* of 2.2×10^{-6} s. This corresponds to a *half life* of 1.52×10^{-6} s, and a *radioactive decay constant* of 0.455×10^6 s^{-1}, thus setting a 'microsecond' timescale over which kinetic processes may be studied using muons. The decay of the muon produces a positron e^+, plus two neutrinos [Eqn (19)]; it is, of course, the positrons which are counted.

$$\mu^+ \rightarrow e^+ + \nu_e + \overline{\nu}_e \qquad (19)$$

$$\pi^+ \rightarrow \mu^+ + \nu_\mu \qquad (20)$$

$$\mu^+ + e^- \rightarrow Mu^\bullet \qquad (21)$$

Although they occur naturally as a consequence of cosmic radiation striking the nuclei of light atoms (*e.g.* O_2, N_2) in the atmosphere, muons are needed in high fluxes for research purposes. Thus they are produced using a particle accelerator, by which means a beam of energised protons is caused to impinge on a beryllium or a carbon target. Among the products of the ensuing nuclear reactions are pions π^+ (binding components of nuclei), which decay on a nanosecond timescale to form muons, as in Eqn (20).

Muonium atoms ($\mu^+ e^-$; Mu) may be formed *in situ* in a range of liquid, solid and gas phase samples, according to Eqn (21), where e^- is a radiolytic electron.

Muonium is equivalent to a normal protium atom (p^+e^-) and indeed shows the chemical properties of a *light* hydrogen atom (Mu has a mass 1/9 that of a protium atom); hence if the sample contains unsaturated organic molecules, Mu can undergo an addition reaction. The method is highly specific for the study of free radicals, of which many types may be so formed. Some examples are indicated in Eqns (22–24):

$$R_2C=CR_2 + Mu^\bullet \rightarrow R_2C^\bullet(Mu)CR_2; \tag{22}$$

$$R_2C=CR–CR=CR_2 + Mu^\bullet \rightarrow R_2C(Mu)–C(R)^\bullet–CR=CR_2; \tag{23}$$

$$R_2C=O + Mu^\bullet \rightarrow R_2C^\bullet–OMu. \tag{24}$$

7.2 Transverse-field muon spin rotation spectroscopy (TF μSR)[65,66]

Though the process outlined above may be viewed in analogy with other isotopic labelling techniques, information equivalent to that obtainable from magnetic resonance experiments[7,8] is also available, because spectroscopic (hyperfine) magnetic interactions (couplings) are revealed by their influence on the positron count rate in designated detectors. Using high magnetic fields, applied transverse (at 90°) to the muon beam direction, the transverse-field muon spin rotation (TF μSR) technique characterises each radical by a single pair of lines, which represent the $-\frac{1}{2}, +\frac{1}{2}$ m_s electron spin combination with the muon (m_μ) states. These occur at the precession frequencies from muons which experience the sum of the applied and ($-\frac{1}{2}, +\frac{1}{2}$ m_s) hyperfine magnetic fields. A classical picture is of the muon spin *rotating* around the axis of the applied magnetic field: rather as the spin of a similar magnetic nucleus, following a 90° *pulse* of radiofrequency radiation in an 'FT NMR' experiment[8] (Section 2.2.2). The muon-electron hyperfine coupling constant is obtained from the difference between the high (v_2) and low (v_1) frequencies for each radical: $A_\mu = v_2 - v_1$. As the coupling increases, for a given magnetic field, the frequency v_2 increases, while concomitantly that m_1 first decreases, reaches zero and then increases once more, due to a sign change in the transition; the coupling is now obtained from the sum of the frequencies: $A_\mu = v_1 - (-v_2)$. A representative example of an actual such TF μSR spectrum is that of radicals (1) derived from DMPO (5,5-dimethyl-1-pyrroline-N-oxide) absorbed as a 30 wt% ethanol solution in silica-gel (Figure 19). Given that single-particle *counting* methods are employed, and the muon spins are nearly 100% polarised (as compared with the Boltzmann factor, on which EPR and NMR depend), techniques involving muons are extremely sensitive (one *single* molecular radical is detected at a time by TF μSR).

7.3 Longitudinal-field muon spin relaxation (LF μSRx)

This technique uses an external magnetic field which is applied in a direction longitudinal with respect to the muon beam direction, and at the Paul Scherrer Institute in Switzerland, both LF μSRx and TF μSR experiments can be performed using the same apparatus: it being a simple matter to physically rotate the magnet
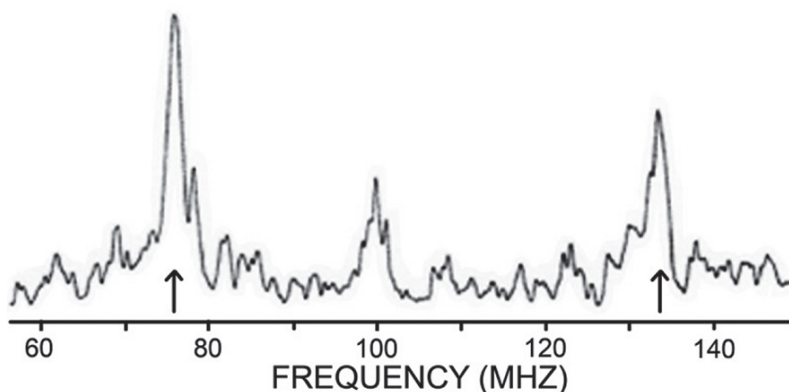
Figure 19 *Transverse-field muon spin rotation (TF μSR) spectrum recorded from radicals (1) sorbed as a 30 wt% ethanol solution in silica-gel at 300 K (see ref. 9).*

through 90° to change the direction of the magnetic field in respect to that of the muon beam[69]. LF μSRx has shown considerable promise in the study of the reorientational rates of radicals sorbed in porous materials, which so far include: zeolites[70–72]; activated carbon[73–75]; silica-gel[67,69,76]; clays[67,69]; and a highly dispersed ice-surface[67]. Though it does not (certainly in its present simple form) approach the level of detail regarding determining molecular reorientation that is possible with ALC-μSR[77,78] (Section 7.4), the method does provide a relatively straightforward estimate of motional correlation times and so of the activation energy associated with a particular kind of motional process.

The physical basis of the method is one of resonance. In general, when the frequency of a particular molecular motion approaches that of the dominant spectral transition (ω) in the muon-electron coupled system[79–81], there is an increase in the relaxation rate (λ) of the muon spins, as measured in a longitudinal magnetic field. This reaches a maximum when the frequencies are equal. Different motional regimes may be identified, and in some cases two maxima are measured (*e.g.* Figure 20), which may reflect two distinct sorbed fractions, each with its own motional characteristics. Motional correlation times (τ) may be estimated from the LF-relaxation rates (λ), *via* Eqn (25):

$$\lambda = (2\pi\delta A)^2 \cdot \tau/(1 + \omega^2\tau^2). \tag{25}$$

In Eqn (25), δA reflects the modulation in the hyperfine frequency during the motional event, which relaxes the muon spin; ω is often taken to be the (angular) frequency of the $|1\rangle \leftrightarrow |2\rangle$ transition ($\omega = 2\pi\nu$), which is strongly induced by the mechanism of motional partial averaging of the anisotropic (dipolar) muon hyperfine coupling, as the radical tumbles[79–81]. Since $\lambda = 1/T_1$, the maximum in the relaxation rate corresponds to a 'T_1 minimum' familiar[7,8] in NMR and EPR spectroscopy. Simple estimates of activation parameters, *viz* inverse-frequency factors (τ_∞) and
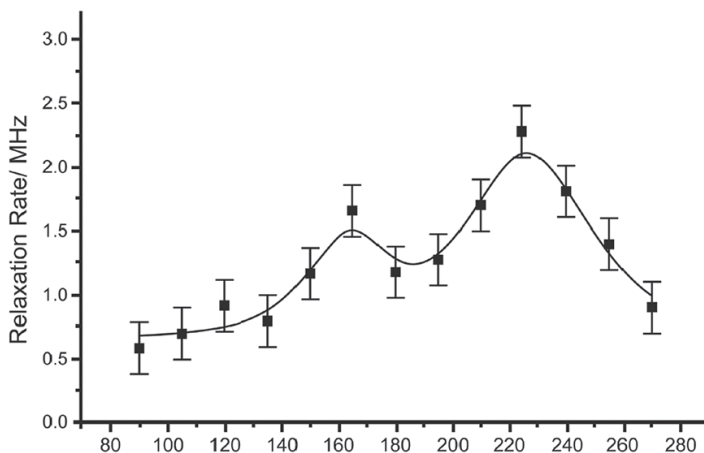
Figure 20 *LF μSRx plot recorded from radicals (1) sorbed as a 30 wt% ethanol solution in silica-gel, showing change in relaxation rate as a function of temperature and that two distinct motional regimes are present[9].*

activation energies (E_a), for internal motion in molecules and for their overall motion in sorbed states, may be made by measuring the muon spin relaxation rate (λ) as a function of temperature. The activation terms (τ_∞) and (E_a) are obtained by fitting the τ values, determined over a particular temperature range, to Eqn (26).

$$\tau = \tau_\infty \exp(E_a/RT) \tag{26}$$

7.3.1 Additional relaxation effects

A number of influences might cause relaxation of the muon spin. At the outset, we note that there will be contributions from transitions other than that between the $|1> \leftrightarrow |2>$ levels; but since this particular transition is strongly induced through the dipolar modulation mechanism which is a feature of molecular reorientation, it is convenient to assume that its (angular) frequency is ω, especially for reorientation on a surface. The choice of frequency will affect the values obtained for the motional correlation times (τ), and hence the inverse-frequency factor, (τ_∞) defined in Eqn (26), but not the activation energy (E_a). Therefore, a plot of $-\ln\tau$ *vs* $1/T$ should provide a meaningful activation energy when a single motional mode is dominant.

Other than the effect of molecular reorientation, the degrees of freedom available to a rigid molecule like cyclohexadienyl are unlikely to affect significantly the muon spin relaxation rate (λ). This is not necessarily true in more flexible structures, which are fairly common in radicals derived by muonium addition to the molecules of volatile organic compounds (VOCs): processes, such as ring-inversion, out-of-plane vibration of a bound muon, and rotation (or torsion) of $MuCH_2$-groups, all modulate the hyperfine coupling of the muon and may cause its relaxation. Paramagnetic centres in the host material are also potential contributors to (λ). Rhodes and his co-workers[70,71] studied a series of cation-exchanged zeolite X samples containing
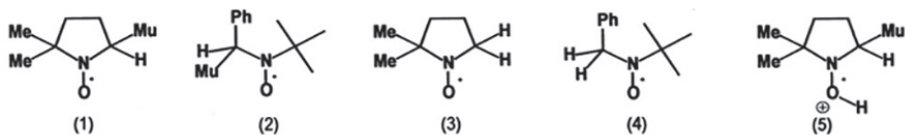
benzene, and used the resulting inverse-frequency factors (τ_∞) and activation energies (E_a) to calculate thermodynamic activation parameters, thus providing a self-consistent set of data for the rigid cyclohexadienyl radical in this medium, reflective of the varying nature of the cation.

7.4 Avoided level crossing (ALC μSR)

As is the case with LF μSRx, this technique uses a magnetic field applied in a direction longitudinal to that of the muon beam. Similarly, the muon spins do not *rotate* (as they do in the TF arrangement) but 'sit' along the magnetic field axis: hence, it is the relaxation (change of spin orientation) of the muon spins that is observed, caused by resonant energy transfer with another magnetic nucleus ($\Delta m = 0$; 'flip-flop' transition), or pure flips of the muon spins ($\Delta m = 1$), induced by fluctuating, anisotropic muon-electron magnetic dipolar couplings. Applications of ALC μSR have been reviewed by Roduner[77,78]. The reader is invited to these reviews and to the papers cited therein for details and applications of the method, whose advantages include the determination of hyperfine coupling constants of magnetic nuclei in the radical, other than the muon itself, and their sign relative to that of the muon hyperfine coupling. From a detailed analysis of the ALC lineshapes, the precise nature of the kind of motion a given radical is undergoing is further revealed, and the method also has particular advantages in studying radicals in the gas phase[9].

7.5 TF μSR, LF μSRx and ALC applied in combination to a single problem

The complementarity and application of the techniques of TF μSR, ALC μSR and LF μSRx, as brought to bear on a single problem, is nicely demonstrated by a study[82] of nitroxyl radicals formed by the addition of muonium to the spin traps DMPO (5,5-dimethyl-1-pyrroline-*N*-oxide) and PBN (*N*-tert-butyl-α-phenylnitrone) sorbed as 30 wt% ethanol solutions in silica-gel. As we have already seen (Section 6.4.1), spin-probes, usually stable nitroxyl radicals, are widely used in the study of molecular reorientational dynamics, as detected by EPR methods. In contrast, studying *reactive* radicals on solid surfaces poses particular difficulties for EPR detection. However, the study of transient radicals is made tractable *via* the suite of methods available for transient radicals which have been labelled with muonium[9]. It is important to connect and compare these distinct approaches. With this aim, the radicals (1) and (2) (Scheme 1) were formed by muonium addition to DMPO (5,5-dimethyl-1-pyrroline-*N*-oxide) and PBN (*N*-tert-butyl-α-phenylnitrone), both prepared as 30 wt% solutions in ethanol and sorbed in silica-gel. Although (1) and (2) are nitroxyl radicals, they are of course not stable radicals since their lifetime is limited by the radioactive decay of the muon (mean lifetime 2.2 μs). This decay permits the detection of (1) and (2), whose structures may be compared with those of chemically similar, sorbed nitroxides determined by EPR[83]. The initial method of detection was TF μSR, the spectrum being as shown in Figure 19 for radicals

Christopher J. Rhodes

Scheme 1

(1) recorded at 300 K; the lines are much broader than expected for a liquid-phase sample, indicating restricted molecular motion. A muon coupling, reduced by the muon/proton magnetogyric ratio (3.1833), of 65.6 MHz may be deduced from the sum of the TF μSR frequencies, in comparison with 57.4 MHz[84] for the *all-proton* isotopomer (3) (Scheme 1), showing an enhancement factor of 1.14 in favour of the muon – in fact a typical value for conformationally restricted radicals[85]. A similar comparison between (2) and (4) (Scheme 1) yields a reduced muon coupling of 29.1 MHz, with an enhancement factor of 1.33: this time typical of conformationally unconstrained radicals[85].

In order to probe further structural details of (1) and (2), avoided level crossing (ALC) measurements were made. An ALC spectrum recorded from radicals (1) at 308 K is shown in Figure 21, displaying *four* resonances, labelled (a)–(d). From each ALC resonance magnetic-field position (B_{res}), possible hyperfine couplings were calculated for ^{14}N and ^1H, according to Eqn (27), in which A_μ and A_k are the couplings to the muon and to the other respective nucleus (^1H, ^{14}N), and γ_μ, γ_k, γ_e are the respective gyromagnetic ratios of the muon, nucleus and electron; M is the total of their spin quantum numbers.

$$B_{res} = (A_\mu - A_k)/2(\gamma_\mu - \gamma_k) - (A_\mu^2 - 2MA_k^2)/2\gamma_e(A_\mu - A_k) \qquad (27)$$

In the case of anisotropic motion, an additional resonance at $A_\mu/2\gamma_\mu$ may be expected[77,78] arising from the pure muon 'spin-flip' transition ($\Delta m = 1$). We assign resonance (a) to the ^{14}N nucleus, for which a coupling of +52.4 MHz is derived. Corresponding to 18.7 G, the coupling is significantly greater than normally encountered for dialkyl nitroxyl radicals, which for both (3) and (4) is 15.6 G as measured in ethanol solution[84]. Resonance (b) yields either a proton coupling of +64.6 MHz using Eqn (1), or a reduced muon coupling of 65.5 MHz ($A_\mu = 2\gamma_\mu$. $B_{res}/3.1833$) assuming it is from the $\Delta m = 1$ transition. In the latter case, the muon coupling agrees exactly with that determined from a TF μSR measurement made at this temperature. Indeed, accord is met over the entire temperature range 285–346 K between the coupling determined by TF μSR and that obtained assuming that the resonance is the pure muon spin-flip transition. Hence we assign it thus, rather than to a proton coupling. The mere observation of this resonance tells that radicals (1) are executing anisotropic reorientational motion. This suggests that there is an interaction between the radicals and the surface of the silica pore which contains them.

Resonances (c) and (d) afford proton couplings of –11.5 and –26.3 MHz. ENDOR studies have been reported on related dialkyl nitroxyl radicals which show
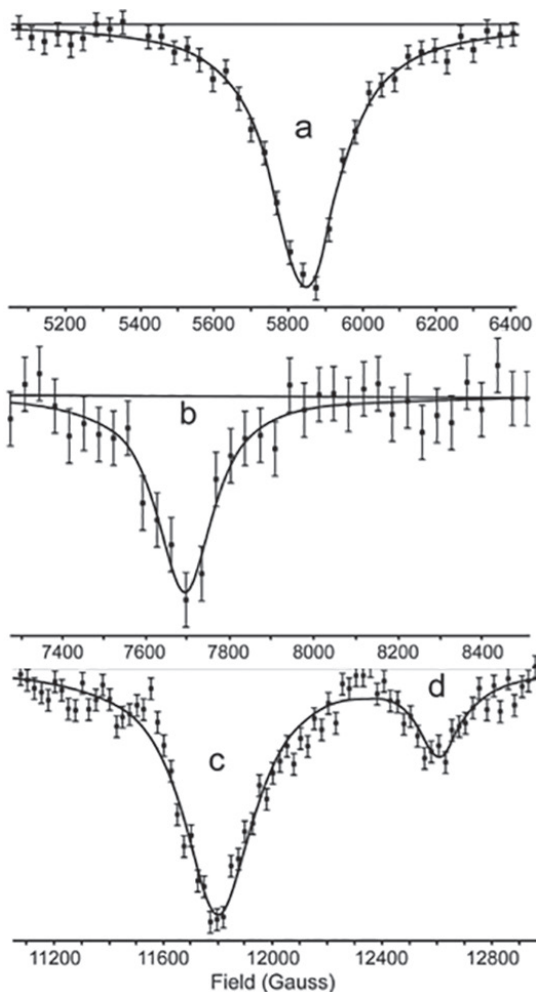
Figure 21 Avoided level crossing (ALC) spectrum recorded at 308 K from (1) sorbed as a 30 wt% ethanol solution in silica-gel, showing four resonances (a)–(d), with relative intensities: 24, 8, 16, 5 (see ref. 9).

that the coupling to the methyl protons is of negative sign[86]. It is therefore tempting to ascribe the –11.5 MHz coupling to the six methyl protons in (1), although the value is much greater than is indicated by ENDOR ($\leq$ 1.6 MHz). The large ^{14}N coupling requires explanation. We note that, at 18.7 G, it far exceeds typical values for dialkyl nitroxyl radicals in protic media[84], and approaches those measured for fully protonated nitroxyls reported by Malatesta and Ingold[87]. We believe this is the crux of the matter, that interaction of (1) or its precursor DMPO with the acidic silica surface leads ultimately to the protonated nitroxide (5) (Scheme 1). H-bonding between (5) and the silica surface would account for the anisotropic reorientation deduced from the $\Delta m = 1$ resonance. [In contrast, (2) has a 'normal'[84] ^{14}N coupling equivalent to 15.9 G, and no $\Delta m = 1$ feature was detected from it.] Since the muon/proton isotope ratio for (5)/(3) is within the normal range[85], there is no evidence that protonation of (1) increases the spin density at the nitrogen atom, which would be expected to

cause an increase in the apparent isotope ratio: more probably, the resulting increase in the electron withdrawing power of the oxygen atom, on protonation, causes a small degree of bending at the N-radical centre, so enhancing the ^{14}N coupling. The resulting increase in σ-character of the singly-occupied molecular orbital then facilitates the transmission of spin-density through the molecular σ-orbital framework, causing an increase in the methyl proton couplings from ca –1.6 MHz to that of –11.5 MHz measured here. It is significant that the proton couplings from the tert-butyl groups in di-tert-butyl nitroxide are increased from +0.077 G[88] to ca (+)0.5 G[87] on protonation in concentrated sulfuric acid. A similar enhancement from –1.6 MHz would give a coupling of ca –10 MHz, which is close to the observed value. The coupling of –26.3 MHz is ascribed to the O–H proton in (5). We had expected to observe additionally a resonance from the unique β-proton in (1)/(5). If the only possible contender, $i.e.$ resonance (b), had in fact been due to this, an unprecedentedly small hyperfine isotope ratio of 1.01 would pertain; given the normal isotope effect of 1.14, noted above for constrained conformations[85], a resonance close to ca 8000 G is actually expected, but as may be judged from the field-scale shown for resonance (b), there is nothing readily apparent.

Longitudinal-field muon spin relaxation (LF μSRx) measurements were next employed. As described in Section 7.3, rotational correlation times were estimated from the relaxation rates measured for these radicals over the temperature range 80–300 K. Two separate motional regimes (Figure 20) were disclosed for both (1) and (2). The appropriate Arrhenius-type plots yielded activation energies of 20.2 ± 2.0 and 11.9 ± 1.5 kJ mol^{-1} for the two kinds of motion identified for (1), but 16.6 ± 1.7 and 4.2 ± 0.3 kJ mol^{-1} for (2). We propose that, in each case, these differences reflect the sorption of radicals at two distinct sites in the silica pores. Some comparisons may be drawn between these results and those reported previously for nitroxyl radicals in ethanol solutions[83] and as sorbed on silica surfaces[89–91], according to EPR measurements. The activation energies are indeed all very similar to those determined using LF μSR, lending confidence to the parity of these widely differing experimental procedures; however, the salient point is that the LF μSR method is applicable to the study of $transient$ radicals in heterogeneous media, which, as noted, is often impossible to do using EPR methods.

8. Conclusions

In the past century and more, since the original observation by Zeeman[2,3,4], that spectral lines can be affected by magnetic fields (and the discovery thereby that intense magnetic fields are present in sunspots), 'magnetic spectroscopy' has evolved into the broad arsenal of techniques known as 'magnetic resonance'. Manifesting themselves primarily as EPR, NMR and μSR, these methods have provided unparalleled insight into the structures, reactivity and dynamics of molecules, and thereby contributed to a detailed basis for much of chemistry, and the environmental and biomedical sciences. MRI scans are now familiar in hospitals, for looking inside the body (complementary to X-ray CT scans), and a $37 billion industry has been

founded on the idea that consuming nutritional supplements is 'good for you', supposedly helping to combat free radicals: reactive molecular species which are understood in detail from their EPR spectra. NMR, EPR and μSR have each been used in materials science investigations of all kinds, and to probe catalytic systems, more recently under their actual working conditions. The list of attainments is very long, but in summary, it is fair to say that our comprehension of the modern world would not be as it is, had the insightful agency of magnetic resonance not been a part of its development.

Published online: 5 August 2017

9. References

1. Cortie, A.L. (1917–1918) *Sci. Prog*., **48**, 282.
2. Zeeman, P. (1897) *Phil. Mag*., **43**, 226.
3. Zeeman, P. (1897) *Phil. Mag*., **44**, 55.
4. Zeeman, P. (1897) *Nature*, **55**, 347.
5. Hale, G.E. (1908) *Astrophys. J*., **28**, 315.
6. Hale, G.E. (1913) *Pop. Sci.*, **83**, 105.
7. Harris, R.K. (1983) *Nuclear magnetic resonance spectroscopy*. Pitman, Melbourne.
8. Carrington, A. and McLachlan, A.D. (1979) *Introduction to magnetic resonance*. Chapman and Hall, London.
9. Rhodes, C.J. (2012) *Sci. Prog.,* **95**, 101.
10. Rabi, I.I., Zacharias J.R., Millman, S., *et al*. (1938) *Phys. Rev*., **53**, 318.
11. Nobelprize.org (n.d.) The Nobel Prize in Physics 1944. https://www.nobelprize.org/nobel_prizes/physics/laureates/1944/ [accessed 3 March 2017].
12. Nobelprize.org (n.d.) The Nobel Prize in Physics 1952. https://www.nobelprize.org/nobel_prizes/physics/laureates/1952/ [accessed 3 March 2017].
13. Zavoisky, E. (1945) *Fizicheskiĭ Zhurnal*, **9**, 211.
14. Kuhn, L.T. (2013) *Hyperpolarization methods in NMR spectroscopy, topics in current chemistry.* Springer-Verlag, Berlin, Heidelberg.
15. Rhodes, C.J. (2011) *Sci. Prog*., **94**, 16.
16. Jacobsen, N.E. (2007) *NMR spectroscopy explained. Simplified theory, applications and examples for organic chemistry and structural biology*. Wiley, Hoboken, New Jersey.
17. Hashi, K., Ohki, S. Matsumoto, S., *et al*. (2015) *J. Mag. Reson*., **256**, 30.
18. Aue, W.P., Bartholdi, E. and Ernst, R.R. (1976) *J. Chem. Phys.*, **64**, 2229.
19. Nobelprize.org (n.d.) The Nobel Prize in Chemistry 1991. https://www.nobelprize.org/nobel_prizes/chemistry/laureates/1991/ [accessed 3 March 2017].
20. Nobelprize.org (n.d.) The Nobel Prize in Chemistry 2002. https://www.nobelprize.org/nobel_prizes/chemistry/laureates/2002/ [accessed 3 March 2017].
21. Hennel, J.W. and Klinowski, J. (2005) Magic angle spinning: a historical perspective. In: Klinowski, J. (ed.), *New techniques in solid-state NMR*, pp. 1–14. Springer-Verlag, Berlin, Heidelberg.
22. Wikipedia (2017) *In vivo* magnetic resonance. https://en.wikipedia.org/wiki/Nuclear_magnetic_resonance_spectroscopy_of_proteins [accessed 3 March 2017].
23. Fürtig, B., Richter, C., Wöhnert, J., *et al*. (2003) *ChemBioChem*, **4**, 936.
24. Addess, K.J. and Feigon, J. (1996) Introduction to ^{1}H NMR spectroscopy of DNA. In: Hecht, S.M. (ed.), *Bioorganic chemistry: nucleic acids*, pp.163–185. Oxford University Press, New York.

25. Wemmer, D. (2000) Structure and dynamics by NMR. In: Bloomfield, V.A., Crothers, D.M. and Tinoco, I. (eds), *Nucleic acids: Structures, properties, and functions*, pp. 111–157. University Science Books, Sausalito, California.

26. Rudin. M. (1992) *In-vivo magnetic resonance spectroscopy*. Springer-Verlag, Berlin, Heidelberg.

27. Jansen, J.F., Backes, W.H., Nicolay, K., *et al.* (2006) *Radiology*, **240**, 318.

28. Saini, K.S., Patel, A.L., Shaikh, W.A., *et al.* (2007) *Singapore Med. J.*, **48**, 783.

29. Mueller-Lisse, U.G. and Scherr, M. (2003) *Der Radiologe,* **43**, 481.

30. Wikipedia (2017) *In vivo* magnetic resonance. https://en.wikipedia.org/wiki/In_vivo_magnetic_resonance_spectroscopy [accessed 3 March 2017].

31. Wikipedia (2017) Functional magnetic resonance spectroscopy of the brain. https://en.wikipedia.org/wiki/Functional_magnetic_resonance_spectroscopy_of_the_brain [accessed 3 March 2017].

32. Branzoli, F., Techawiboonwong, A., Kan, H., *et al.* (2012) *Magn. Reson. Med.*, **69**, 303.

33. Gussew, A., Rzanny, R., Erdtel, M., *et al.* (2010) *NeuroImage*, **49**, 1895.

34. Prichard, J., Rothman, D., Novotny, E., *et al.* (1991) *Proc. Natl Acad. Sci. USA*, **88**, 5829.

35. Rink, P.A. (2017) What is the organ distribution of MRI studies? http://www.magnetic-resonance.org/ch/21-01.html [accessed 3 March 2017].

36. Smith-Bindman, R., Miglioretti, D.L., Johnson, E., *et al.* (2012) *JAMA*, **307**, 2400.

37. Wikipedia (2017) Magnetic resonance imaging. https://en.wikipedia.org/wiki/Magnetic_resonance_imaging [accessed 3 March 2017].

38. American College of Radiology (2013) ACR–ASNR–SPR practice parameter for the performance and interpretation of magnetic resonance imaging (MRI) of the brain. https://www.acr.org/~/media/ACR/Documents/PGTS/guidelines/MRI_Brain.pdf [accessed 3 March 2017].

39. Nolen-Hoeksema, S. (2014) *Abnormal psychology,* 6th edition, p. 67. McGraw-Hill Education, New York.

40. ACCF/ACR/SCCT/SCMR/ASNC/NASCI/SCAI/SIR (2006) Appropriateness criteria for cardiac computed tomography and cardiac magnetic resonance imaging. *J. Amer. Coll. Radiol*., **3**, 751.

41. Husband, J. (2008) Recommendations for cross-sectional imaging in cancer management. https://www.rcr.ac.uk/publication/recommendations-cross-sectional-imaging-cancer-management-second-edition [accessed 11 May 2017].

42. Zijta, F.M., Bipat, S. and Stoker, J. (2010) *Eur. Radiol*., **20**, 1031.

43. Elster, A.D. (2017) Relaxation rates *vs* times. http://mriquestions.com/relaxation-rate-vs-time.html [accessed 11 May 2017].

44. Atkins, P.W. (1986) *Physical chemistry,* 3rd edition, p. 495. Oxford University Press, Oxford.

45. Wikipedia (2017) Relaxation (NMR). https://en.wikipedia.org/wiki/Relaxation_(NMR) [accessed 3 March 2017].

46. Rhodes, C.J. (2011) *Sci. Prog*., **94**, 339.

47. Dobbs, A.J. (1974) *Electron spin resonance,* Vol. 2*, Chem. Soc. Specialist Periodical Reports,* p. 281*.* The Chemical Society, London.

48. Rhodes, C.J. (1999) *Toxicology of the human environment: the critical role of free radicals*. Taylor and Francis, London.

49. Wikipedia (2017) Electron paramagnetic resonance - cite note-lowd-6. http://en.wikipedia.org/wiki/Electron_paramagnetic_resonance#cite_note-lowd-6 [accessed 3 March 2017].

50. Swartz, H.M., Khan, N., Buckey, J., *et al.* (2004) *NMR Biomed.*, **17**, 335.

51. Wikipedia (2017) Pulsed electron paramagnetic resonance. https://en.wikipedia.org/wiki/Pulsed_electron_paramagnetic_resonance [accessed 3 March 2017].

52. Schweiger, A. and Jeschke, G. (2001) *Principles of pulse electron paramagnetic resonance*. Oxford University Press, Oxford.

53. Eaton, S.S. and Eaton, G.R. (2009) *Concepts Magn. Reson*., **34A**, 315.

54. Berliner, L.J. (ed.) (1976) *Spin-labelling: theory and applications*. Academic Press, New York.

55. Knowles, P.F. and Marsh, D. (1991) *Biochem. J.*, **274**, 625.

56. Marsh, D. and Horvath, L.I. (1989) Advanced ESR. In: Hoff, A.J. (ed.), *Applications in biology and biochemistry*, p. 707. Elsevier, Amsterdam.
57. Van Bilsen, D.G.J.L. and Hoekstra, F.A. (1993) *Plant Physiol*., **101**, 675.
58. Cassol, R., Ge, M.T., Ferriani, A. and Freed, J.H. (1997) *J. Phys. Chem*., **101**, 8782.
59. Patyal, B.R., Crepeau, R.H. and Freed, J.H. (1997) *Biophys. J.*, **73**, 2201.
60. Xu, D.J., Crepeau, R.H., Ober, C.K. and Freed, J.H. (1996) *J. Phys. Chem,* **100**, 15873.
61. Marsh, D. (1997) *Eur. Phys. J. Biophys.*, **26**, 203.
62. Swamy, M.J. and Marsh, D. (1997) *Biochemistry*, **36**, 7403.
63. Marsh, D. (1996) *Braz. J. Med. Biol. Res.*, **29**, 863.
64. Smirnov, A.I., Smirnova, T.I. and Morse, P.D. (1995) *Biophys. J.*, **68**, 2350.
65. Walker, D.C. (1983) *Muon and muonium chemistry*. Cambridge University Press, Cambridge.
66. Roduner, E. (1988) *The positive muon as a probe in free radical chemistry. Lecture notes in chemistry*. Springer, Heidelberg.
67. Rhodes, C.J. (2012) Applications of EPR in the environmental sciences. In: Lund, A and Shiotani, M. (eds), *EPR of free radicals in solids: trends in methods and applications,* 2nd edition, pp. 279–310. Springer, Dordrecht.
68. Wikipedia (2017) Tritium. http://en.wikipedia.org/wiki/Tritium [accessed 3 March, 2017].
69. Rhodes, C.J., Dintinger, T.C., Reid, I.D. and Scott, C.A. (2000) *Magn. Reson. Chem.,* **38**, 281.
70. Rhodes, C.J., Dintinger, T.C. and Scott, C.A. (2000) *Magn. Reson. Chem*., **38**, 62.
71. Rhodes, C.J., Dintinger, T.C. and Scott, C.A. (2000) *Magn. Reson. Chem.*, **38**, 729.
72. Rhodes, C.J. and Dintinger, T.C. (2011) *Prog. React Kinet. Mech.*, **36**, 287.
73. Rhodes, C.J. and Reid, I.D. (2002) *Spectrochimica Acta A,* **58**, 1209.
74. Rhodes, C.J., Dintinger, T.C., Reid, I.D., *et al*. (2000) *Magn. Reson. Chem*., **38**, S58.
75. Rhodes, C.J. (2006) *Prog. React. Kinet. Mech*., **31**, 159.
76. Rhodes, C.J., Reid, I.D. and Zimmermann, U. (2002) *Chem. Comm*., 1092.
77. Roduner, E. (1993) *Chem. Soc. Rev.*, **22**, 337.
78. Roduner, E., Schwager, M. and Shelley, M. (1995) Muon spin resonance of radicals on surfaces. In: Lund, A. and Rhodes, C.J. (eds), *Radicals on surfaces,* pp. 259–276. Kluwer, Dordrecht.
79. Cox, S.F.J. (1998) *Solid State Nucl. Magn. Reson*., **11**, 103.
80. Cox, S.F.J. and Sivia, D.S. (1997) *Appl. Magn. Reson*., **12**, 213.
81. Christides, C., Cox, S.F.J., David, W.I.F., *et al*. (1993) *J. Chim. Phys.,* **90**, 663.
82. Rhodes, C.J., Reid, I.D. and Zimmermann, U. (2002) *Chem. Comm*., 1092.
83. Mazzoleni, F., Ottaviani, M.F., Romanelli, M., *et al*. (1988) *J. Phys. Chem*., **92**, 1953.
84. Buettner, G. (1987) *Free Radic. Biol. Med*., **3**, 259.
85. Rhodes, C.J and Symons, M.C.R. (1988) *J. Chem. Soc., Faraday Trans. 1*, **84**, 1187.
86. Poole, C.P. and Farach, H.A. (1994) *Handbook of electron spin resonance,* p. 371. AIP Press, New York.
87. Malatesta, V. and Ingold, K.U. (1973) *J. Am. Chem. Soc*., **95**, 6404.
88. Petillo, P.A., De Felippis, J. and Nelsen, S.F. (1991) *J. Org. Chem*., **56**, 6496.
89. Rhodes, C.J. and Lund, A. (1995) *Radicals on surfaces*, p. 259. Kluwer, Dordrecht.
90. Lozos, G.P. and Hoffmann, B.M. (1974) *J. Phys. Chem*., **78**, 2110.
91. Golubev, V.B., Lunina, E.V. and Selivanovskii, A.K. (1981) *Russ. Chem. Rev*., **50**, 421.
92. Gigandet, X., Hagmann, P., Kurant, M., *et al*. (2008) *PLoS ONE*, **3**, e4006.
93. Rhodes, C.J (1997) Electron spin resonance studies of peroxyl radicals in solid matrices. In: Alfassi, Z. (ed.), *Peroxyl radicals*, pp. 335–354. Wiley, Chichester.
94. Rhodes, C.J. and Dintinger, T.C. (1999) ESR studies of lipids. In: Hamilton, R. and Cast, J. (eds), *Spectral properties of lipids*, pp. 270–306. Wiley–Blackwell, New York.